The E3 ligase adapter cereblon targets the C-terminal cyclic imide degron

The E3 ubiquitin ligase adaptor cereblon targets the C-terminal cyclic imide degron

Authors: Saki Ichikawa,*,† Hope A. Flaxman,*,† Wenqing Xu,*,† Nandini Vallavoju,† Hannah C. Lloyd,† Binyou Wang,# Dacheng Shen,† Matthew R. Pratt,# Christina M. Woo†

Affiliations:

* These authors contributed equally to this work

† Department of Chemistry and Chemical Biology, Harvard University, Cambridge, MA 02138

Department of Chemistry and Biological Sciences, University of Southern California, Los Angeles, CA 90089

Abstract: The E3 ligase substrate adaptor cereblon (CRBN) is a target of thalidomide and lenalidomide,[1] which are therapeutic agents used in the treatment of hematopoietic malignancies[2-4] and as ligands for targeted protein degradation.[5-7] These agents are proposed to mimic a naturally occurring degron; however, the structural motif recognized by the thalidomide-binding domain of CRBN is unknown. Here, we report that C-terminal cyclic imides, overlooked post-translational modifications that arise from intramolecular cyclization of glutamine or asparagine residues, are physiological degrons on substrates for CRBN. Dipeptides bearing the cyclic imide degron are substitutes for thalidomide when embedded within bifunctional chemical degraders. Installation of the degron to the C-terminus of proteins induces CRBN-dependent ubiquitination and degradation in vitro and in cells. C-Terminal cyclic imides form adventitiously on physiologically relevant timescales throughout the human proteome to afford a degron that is endogenously recognized and removed by CRBN. The discovery of the C-terminal cyclic imide degron defines a novel regulatory process that may impact the physiological function and therapeutic engagement of CRBN.

Main Text:

Cereblon (CRBN) is a conserved protein that functions as a substrate recognition adaptor in the $CRL4^{CRBN}$ E3 ubiquitin ligase complex. The immunomodulatory drugs (IMiDs) thalidomide, lenalidomide, and pomalidomide bind CRBN and modulate the selection of protein substrates for ubiquitination and degradation,[1] which partially underlies the pleiotropic effects of the IMiDs, including their therapeutic efficacy in multiple myeloma,[2,3] del(5q) myelodysplastic syndrome,[4] and the teratogenic effects observed during development.[8-10] However, the endogenous substrate selection mechanisms of CRBN have remained elusive. The conservation of CRBN across species[11] and its association with neurological development[12] implies its participation in a vital biological process that may be impacted during therapy.

E3 ubiquitin ligase complexes select proteins for degradation through the recognition of degrons, specific amino acid sequences embedded in a substrate that promote ubiquitination and degradation. Short sequences at the protein N-terminus were the first discovered degrons[13] and E3 ligases that recognize C-terminal degrons have recently been reported.[14] Degrons may also be generated by post-translational modifications (PTMs), such as the recognition of proline oxidation by the E3 ligase VHL.[15] Additionally, small molecules that chemically-induce degrons exist in nature (*e.g.*, the plant hormone auxin), which are reminiscent of the activity of the IMiDs.[16] Therefore, IMiD-based degraders may chemically mimic the endogenous recognition element of the thalidomide-binding domain of CRBN by one of these mechanisms (**Fig. 1a**).

Efforts to identify a degron for the thalidomide-binding domain of CRBN have sought to either discover substrates that compete for IMiD binding or reveal ligands by an in vitro structure-focused approach. Substrates for the thalidomide-binding domain of CRBN that compete for binding with thalidomide include MEIS2[17] and amyloid precursor protein,[18] yet a degron within these substrates has not been identified. Structure-focused approaches capitalize on the finding that thalidomide binds to CRBN by creating contacts through the glutarimide ring,[17,19] which suggests that the degron recognized by CRBN could derive from nucleotide or amino acid sources with the potential for a similar binding pattern (**Fig. 1b**). Although several uridine derivatives can bind to the thalidomide-binding domain of CRBN in vitro,[20,21] limited connection of these ligands to cellular activity has been reported. We hypothesized that thalidomide may mimic PTMs like pyroglutamate or C-terminal cyclic imides that arise from cyclized glutamine (cQ) or cyclized asparagine (cN) (**Fig. 1b, Extended Data Fig. 1a**). These PTMs are generated by enzymes,[22] spontaneous cyclization during protein aging,[23-26] or during specific protein splicing events (*e.g.*, intein excision).[27-29] C-Terminal cyclic imides may therefore be overlooked PTMs if proteins bearing these modifications are indeed recognized and degraded by CRBN.

Substitution of IMiDs in degraders

A major challenge to the discovery of a physiologically relevant degron for the thalidomide-binding domain of CRBN is the identification of a minimal functional chemical motif from a vast array of potential cellular substrates. To circumvent this challenge, we first set out to identify biomimetic ligands that functionally engage CRBN using a targeted protein degradation strategy[30] to report on engagement of CRBN in the $CRL4^{CRBN}$ complex in cells. Inspired by the flexible conversion of the bromodomain BRD4 inhibitor JQ1 into a BRD4 degrader by functionalization with a thalidomide analog (*e.g.*, dBET6),[5-7] we designed analogous degraders that replaced thalidomide with potential biomimetic ligands for CRBN (**Fig. 1c**). We expected that successful

substitution of thalidomide with a biologically relevant structure would promote degradation of BRD4 and thus give a functional readout for CRBN engagement in cells.

Surprisingly, our initial evaluation of uridine-based or pyroglutamate probes revealed no functional engagement of CRBN leading to degradation of BRD4 (**Extended Data Fig. 1b–e**). Ensuing evaluation of 15 candidates eventually revealed a set of functional degraders consisting of JQ1 linked to a dipeptide with a C-terminal glutarimide (JQ1-XcQ, **Fig. 1c**). Degradation of BRD4 with JQ1-XcQ minimally requires the dipeptide motif for functional engagement of CRBN (**Extended Data Fig. 1d–e**). Substitution of the dipeptide degrader at the variable N–1 position (X) with each of the twenty amino acids showed that all of the dipeptide degraders promoted degradation of BRD4 in a dose-dependent manner (1 nM–10 μM), with the exception of JQ1-DcQ and JQ1-EcQ, and that non-polar and aromatic amino acid side chains promoted the most efficient degradation (**Fig. 1d**, **Extended Data Fig. 2a**). Interestingly, the hook effect resulting in reduced degradation of BRD4 can be observed from dBET6 at 10 μM, but not from the dipeptide degraders.

Based on these data and molecular similarity to thalidomide, the dipeptide FcQ was selected for further evaluation. Treatment of HEK293T wild-type (WT) or CRBN knockdown (CRBN KD) cells[31] with dBET6 or JQ1-FcQ showed that degradation of BRD4 was CRBN-dependent (**Fig. 1e**). Epimerization of JQ1-FcQ at each of the three stereocenters (in JQ1, Phe, or cQ) inactivated the degrader, indicating that the natural stereochemistry of the amino acids promotes optimal recognition by CRBN and degradation of BRD4 (**Fig. 1f**). The addition of lenalidomide or Boc-protected FcQ (Boc-FcQ) competitively inhibited BRD4 degradation by JQ1-FcQ or dBET6, indicating that the thalidomide-binding domain of CRBN is engaged by glutarimide ligands (**Fig. 1g, Extended Data Fig. 2b**). Both degraders similarly depleted BRD4 within 90 min in a Cullin-dependent manner (**Extended Data Fig. 2c**). Collectively, these data establish glutarimide-based dipeptides are successful substitutes for thalidomide and functionally engage CRBN in cells.

We also evaluated whether the aspartimide, a second class of cyclic imides derived from asparagine, is a functional substitute of thalidomide, given their chemical similarity and the reported formation of C-terminal aspartimides in long-lived proteins or from protein splicing products (*e.g.*, inteins), which are typically promoted by a penultimate histidine. We constructed aspartimide-based dipeptide degraders for evaluation in BRD4 degradation assays in cells (**Fig. 1c**). We synthesized JQ1-XcN degraders embedded with Phe, Leu, and His at the N–1 position (X) and observed degradation of BRD4 by the aspartimide-based dipeptide degraders comparable to that with glutarimide-based dipeptide degraders (**Fig. 1h**, **Extended Data Fig. 2d**). Closer investigation of JQ1-FcN showed that degradation of BRD4 by JQ1-FcN was dependent on CRBN, completed within 2 h in HEK293T cells, and competitively inhibited by lenalidomide and the dipeptide Boc-FcN (**Fig. 1h, Extended Data Fig. 2e–g**). These data indicate that aspartimide-based dipeptides are analogous to glutarimide-based dipeptides in terms of their cellular engagement of CRBN. We thus focused our efforts on further characterization of both 5- and 6-membered C-terminal cyclic imides as degrons recognized by CRBN.

Dipeptide degraders are ligands for CRBN

We next investigated the propensity of the different degraders to directly engage CRBN and mediate ternary complex formation with BRD4, as cellular degradation of BRD4 by chemical degraders is a composite of cellular accessibility, ternary complex engagement, and orientation of the complex for ubiquitination,[7,32] all of which may influence the effective degradation efficiency. The target protein BRD4 was co-immunoprecipitated by FLAG-CRBN from a stable HEK293T

cell line (HEK-CRBN)[31] upon treatment with dipeptide degraders with a range of activities (*e.g.*, JQ1-FcQ, JQ1-FcN, JQ1-DcQ, JQ1-EcQ), indicative of successful engagement of CRBN in cells (**Extended Data Fig. 3a**). These data imply that CRBN has a broad and flexible ligand scope for C-terminal cyclic imide ligands.

To directly evaluate the engagement of CRBN, we used photo-lenalidomide[33] to perform a photo-affinity labeling displacement assay with CRBN/DDB1 (**Extended Data Fig. 3b–d**). Significant displacement was measured with lenalidomide, the dipeptides (FcQ, FcN, DcQ), and a pentapeptide GGGFcQ, but not a dipeptide bearing pyroglutamate (FpE). By contrast, displacement by uridine metabolites was not generalizable.

Subsequently, we evaluated the ternary complex mediated by the dipeptide degraders with recombinant GST-BRD4 and His-CRBN/DDB1 using an AlphaScreen, which produces a signal if the degrader recruits GST-BRD4 and His-CRBN/DDB1 into close proximity (**Extended Data Fig. 4a**) We found that all of the dipeptide degraders induced ternary complex formation and the relative area under the curve reflected the cellular degradation trends, with several of the dipeptide degraders resulting in a signal greater than or comparable to dBET6 (**Fig. 2a, Extended Data Fig. 4b**). The aspartimide-based degraders induced comparable ternary complex formation to the analogous glutarimide-based degraders, in alignment with BRD4 degradation observed in cells. Interestingly, the inactive degrader JQ1-cQ promotes ternary complex formation equivalent to the active JQ1-GcQ, indicating that the N–1 amino acid residue positions the ternary complex in a more productive conformation. Measurement of ternary complex formation in cells using a NanoBRET assay revealed similar trends (**Extended Data Fig. 4d–e**). In sum, these data illustrate that all of the dipeptide degraders directly engage CRBN in vitro and in cells and that the efficiency of ternary complex formation broadly corresponds with the observed cellular activity.

Substrate recruitment by CRBN ligands

We next investigated whether the cyclic imide-containing dipeptides can chemically-induce substrate recruitment for ubiquitination by the $CRL4^{CRBN}$ E3 ligase complex, which would be analogous to the mechanism of thalidomide and derivatives (**Fig. 1a**). To predict whether the dipeptides would recruit substrates through a beta-hairpin motif similar to thalidomide,[34] we performed molecular modeling with the dipeptide degraders in the ternary complex with CRBN, dBET6, and BRD4 (**Extended Data Fig. 5a**). These models indicated that the imide region of the dipeptide binds to CRBN in a similar manner as thalidomide, but the amino acid at the N–1 position occupies a distinct molecular space relative to the phthalimide region of thalidomide. The dipeptides are therefore unlikely to stabilize the same beta-hairpin motifs as the IMiDs but may mediate interactions with unique substrates. We thus co-immunoprecipitated CRBN from HEK-CRBN cells overexpressing IKZF1 in the presence of pomalidomide, FcQ, FcN, or a longer peptide GGGFcQ, but found that no additional substrates significantly co-immunoprecipitated with any of the evaluated peptide ligands (**Fig. 2b–c, Extended Data Fig. 5b–d, Supplementary Information Table 1**).

To evaluate whether the peptides independently promote substrate degradation in cells, we examined the minimal motif necessary for competitive inhibition of BRD4 degradation by JQ1-FcQ in cells and found that the Boc-protected dipeptide (Boc-FcQ) was the most effective competitor (**Extended Data Fig. 5e**). Although the Boc-protecting group is bulky, we treated the multiple myeloma cell line MM.1S with 10 μM of pomalidomide or a dipeptide (Boc-FcQ, Boc-FcN) for 10 h and evaluated potential substrates by global proteomics. Treatment with

pomalidomide showed selective degradation of IKZF1, but no examined substrates consistently showed a change in level upon treatment with either Boc-FcQ or Boc-FcN (**Fig. 2d–f, Extended Data Fig. 5f, Supplementary Information Table 2**).[2,3] IKZF1 expression levels were similar across treatments (**Extended Data Fig. 5g**). The differences in substrate degradation extended to differences in anti-proliferative effects, as MM.1S cells were sensitive to lenalidomide treatment (IC_{50} = 31.6 μM), but not to Boc-FcQ or Boc-FcN (IC_{50} > 100 μM, **Fig. 2g**). The absence of independent substrate degradation observed with Boc-FcQ translated to high target protein selectivity in depleting BRD2 and BRD4 from the degrader JQ1-FcQ (**Extended Data Fig. 5h, Supplementary Information Table 2**). Protein expression levels of BRD2 and BRD4 were similar across treatments (**Extended Data Fig. 5i**). Taken together, these data indicate that the peptide ligands examined here do not engage or degrade chemically induced substrates in vitro or in MM.1S or HEK293T cells.

C-Terminal imides are substrates for CRBN

To characterize whether the dipeptides FcQ and FcN behave as a degron following incorporation into a protein substrate, we used the sortase system[35] to install a C-terminal cyclic imide to GFP-LPETG-His_6 and afford semi-synthetic GFP bearing C-terminal cyclic imide motifs (*e.g.*, GFP-FcQ or GFP-FcN, **Fig. 3a**). We also engineered controls, including GFP-GGG, GFP-Me with an inactive methylated glutarimide, and GFP-FQ and GFP-FN bearing the parent uncyclized amino acid.

The engineered GFPs were evaluated as substrates for the $CRL4^{CRBN}$ complex by examining their susceptibility to the priming step of ubiquitination in vitro. The $CRL4^{CRBN}$ complex isolated from HEK-CRBN cells selectively transferred lysine-free (K0) ubiquitin to GFP-FcQ and GFP-FcN and was competitively inhibited by co-treatment with lenalidomide (**Fig. 3b–c**). By contrast, GFP-FQ and GFP-FN were not modified by the $CRL4^{CRBN}$ complex, indicating that the cyclic imide is required (**Fig. 3d–e**).

We further assessed whether the cyclic imide is a degron for CRBN in cells by introducing the modified GFPs into HEK293T cells by electroporation. Analysis of cellular GFP levels after 6 h revealed significantly lower GFP levels when GFP-FcQ or GFP-FcN was delivered to cells relative to GFP-Me (**Fig. 3f**). The rapid degradation of GFP-FcQ and GFP-FcN was commuted on genetic knockout of CRBN, cotreatment with lenalidomide, or electroporation of GFP-FQ or GFP-FN (**Fig. 3f–h**). The sequence specificity of the C-terminal cyclic imide degron and its activity across cell lines and species were also evaluated. Tailoring of the C-terminus of GFP with PcQ, LcQ, or LcN accelerated depletion of GFP relative to GFP-His_6 in HEK293T cells, which was rescued by lenalidomide competition (**Fig. 3i**). Depletion of GFP bearing a C-terminal cyclic imide was additionally observed across cell lines (Jurkat cells) and species [mouse embryonic fibroblast cells (MEF), **Fig. 3j–k**]. These data indicate that recognition of the C-terminal cyclic imide degron by CRBN is conserved across cell types and species and that CRBN flexibly accepts various amino acid residues adjacent to the cyclic imide.

Transferability of the cyclic imide degron

If thalidomide is mimicking the C-terminal cyclic imide degron, we would expect the degron to readily substitute thalidomide in separate small molecule degraders and proteins. The thalidomide moiety of the degrader dFKBP-1[5] was readily substituted with FcQ to afford and active dFKBP-

FcQ, which degraded the target protein FKBP12 in a CRBN-dependent manner (**Extended Data Fig. 6a–d**). The pomalidomide moiety of a third degrader, dCDK6-Pom,[36] was also readily substituted with FcQ to afford the active CDK6 degrader, dCDK6-FcQ (**Fig. 6e–g**). Furthermore, the cyclic imides were transferrable degrons that promoted ubiquitination and degradation of GST-FKBP12 as a separate engineered substrate at the thalidomide-binding domain of CRBN in vitro and in cells (**Extended Data Fig. 6h–k**). These data demonstrate that the dipeptide FcQ is a transferrable chemical motif and that cyclic imides are genuine degrons of CRBN that promote degradation of proteins bearing this modification at the C-terminus in cells.

C-Terminal cyclic imides are frequent PTMs

We next sought evidence for the natural occurrence of C-terminal cyclic imide PTMs in the proteome. Cyclic imides are formed spontaneously during asparagine or glutamine deamidation and an analogous process wherein nucleophilic attack from the amide side chain results in protein cleavage and reveals the degron for CRBN (**Fig. 4a**). Although cyclic imides undergo subsequent hydrolysis, we found that C-terminal cyclic imides have half-lives at 37 °C in PBS ($t_{1/2}$ cQ = 18.4 h, $t_{1/2}$ cN = 16.7 h; $t_{1/2}$ GFP-FcQ = 24.9 h, $t_{1/2}$ GFP-FcN = 23.0 h) well within the degradation timeframe of most known substrates of CRBN induced by the IMiDs (2–8 h in cells, **Extended Data Fig. 7a**).

The relatively long half-lives of these modifications indicate their availability for recognition by CRBN and that the actual prevalence of C-terminal cyclic imide PTMs in the cellular proteome may be higher than previously recognized. Spontaneous formation of C-terminal cyclic imides has been most prevalently observed with inteins, which promote excision through a specific protein fold.[37] However, examination of two inteins in vitro and in cells indicated that these proteins are not generally a source of CRBN substrates, which may be due to the hindered C-terminus resulting from intein excision (**Extended Data Fig. 7b–f**). To detect where these modifications may be occurring in human proteomes, we analyzed large global proteomics datasets from the NCI7 cell line panel and six primary human tissues for C-terminal cyclic imides collected by the Clinical Proteomic Tumor Analysis Consortium (CPTAC).[38-44] We identified several hundred proteins with over one thousand unique sites of cN or cQ modification across these datasets (**Fig. 4b, Supplementary Information Table 3**). These modification sites occurred at a rate of 0.8% relative to the fully tryptic peptides by spectral counting in the NCI7 dataset. Sequence alignment of these modification sites revealed an apparent consensus sequence that was distinct from the sequence alignment of any N or Q site in the proteome (**Fig. 4c**). As C-terminal cyclic imides may hydrolyze during sample processing, we additionally searched for semi-tryptic peptides with C-terminal N or Q that may represent spontaneous cyclic imide cleavage sites and found over 20,000 putative cleavage sites derived from 6,800 proteins (**Extended Data Fig. 8a, Supplementary Information Table 3**). Mapping the most frequently observed C-terminal cyclic imide modification sites to protein structure indicates that these sites are largely solvent-exposed.

We noted that C-terminal cyclic imides derived from hemoglobin subunits alpha and beta were two of the most frequently observed proteins by spectral counting in our analyses, with a total of eight unique cN or cQ modification sites identified across the global proteomics datasets. Hemoglobin is globally expressed across tissue types, but is particularly abundant in red blood cells, which have a lifespan of approximately 120 days, but do not express CRBN.[45] Therefore, cyclic imides formed on hemoglobin may accumulate and not be degraded in vivo. Indeed, CRBN was not observed in red blood cells by proteomics or Western blot (**Extended Data Fig. 8b**). To

confirm the existence of cN and cQ modifications, we digested recombinant HBB with trypsin at 47 °C for 1 h and mapped six cN and cQ sites across the protein, including cN58, cQ128, and cQ132, which were also observed in the CPTAC global proteomics analysis (**Fig. 4d**). A similar evaluation of red blood cell lysates from two healthy donors revealed three unique peptides bearing a C-terminal cN modification that appeared at retention times independent of the parent tryptic peptide and were fully responsive to base treatment performed prior to mass spectrometry analysis, which induces hydrolysis of the C-terminal cyclic imide (**Fig. 4d, Extended Data Fig. 8c–e, Supplementary Information Table 4**). Digestion of red blood cell lysates with the orthogonal protease chymotrypsin revealed two modification sites on HBA that were also observed in the CPTAC global proteomics datasets (HBA cN79, HBA cQ55) (**Fig. 4d, Extended Data Fig. 8d, f**). These data indicate that C-terminal cyclic imides are present in authentic human samples and not formed during mass spectrometry sample preparation or analysis.

To further extend the observation of C-terminal cyclic imides in aged proteins, we obtained bovine eye lenses as crystallins are known to undergo deamidation to afford cyclic imide modifications during aging, leading to their structural instability and aggregation.[46,47] We mapped 22 modification sites, mostly on beta-crystallins, that were responsive to base treatment and differentiable from the corresponding tryptic peptides by their different retention times (**Extended Data Fig. 8h–i, Supplementary Information Table 4**). The identification of over a thousand cN and cQ modification sites across proteins in human tissues, red blood cells, and bovine eye lenses dramatically expands the map of these modifications in the human proteome and implies that they are more prevalent than previously understood.

Formation of the cyclic imide degron

To verify the ready formation of C-terminal cyclic imide modifications, we evaluated three synthetic peptides from proteins bearing four of the most frequently observed modification sites: HBB[42–60], HBA[63–91], and ACTB[96–113] (highlighted in red and blue, **Fig. 4d**). These peptides were monitored for internal cleavage and formation of the C-terminal cyclic imide, followed by downstream hydrolysis at 37 °C, over a pH range of 7.4–9.0 (**Extended Data Fig. 9a**). The fragmentation spectra from the synthetic peptides and their cleavage products were only identical to those assigned by global proteomics. Furthermore, the extracted ion chromatograms for the parent peptide, the cyclic imide-bearing fragment, and its hydrolyzed products all showed distinct retention times, apart from the cyclic imide fragment at HBA cN79 where the hydrolysis product HBA N79 was readily measured (**Extended Data Fig. 9b**). The spontaneous formation of the cyclic imide fragment was observed from each peptide after 24 h and largely plateaued after 48 h. In contrast, the abundance of the hydrolyzed forms of the cyclic imide fragment for all four sites continuously increased over 10 d in a pH-dependent manner (**Fig. 4e, Extended Data Fig. 9c–e, Supplementary Information Table 5**).

We next investigated the rate of formation of HBB cN58 on recombinant HBB using selected ion monitoring (SIM). To generate the internal standard, the synthetic heavy HBB[42*–60] was incubated at 37 °C for 48 h to form HBB[42*–cN58] and HBB[42*–N58]. We found that recombinant HBB possessed 0.10% of HBB cN58 and 0.15% of HBB N58, which increased on incubation to amounts analogous to that observed with the HBB[42–60] peptide (**Fig. 4f–g**). The levels of the modification observed in vitro are approximately 10-fold greater than that observed from RBC digests, where the full hemoglobin complex is presumably intact (**Fig. 4h, Extended Data Fig. 8g, 9f**). Collectively, although for any individual peptide or protein sequence, the C-

terminal cyclic imide concentration may plateau at a low level, the gradual increase of the corresponding hydrolyzed fragments will accumulate significantly over time if there is no mechanism for removal of protein fragments bearing the C-terminal cyclic imide.

Regulation of cyclic imides by CRBN

The global increase in C-terminal cyclic imide modifications observed across a range of proteins following loss or competitive inhibition of CRBN would align with a protein damage or aging mechanism that generates these modifications. To demonstrate that a protein bearing an adventitiously formed cN or cQ modification affords a degron recognized by the thalidomide-binding domain of CRBN, we examined frequently measured modification sites from the CPTAC global proteomics analyses for compatibility with expressed protein ligation and selected recombinant HBB[1–cQ132] for closer analysis. The degron-modified HBB[1–cQ132] and the methylated control HBB[1–Me132] was prepared via a ligation and deselenization sequence (**Fig. 5a, Extended Data Fig. 10a**). Subjection of HBB[1–cQ132] to in vitro ubiquitination with lysine-free (K0) ubiquitin in the presence of the $CRL4^{CRBN}$ complex showed enhancement of di- and tri-mono-ubiquitination events in a manner that is inhibited by lenalidomide or methylation of the degron (**Fig. 5b, Extended Data Fig. 10b**). These ubiquitination events mapped to K[66, 67] (modified at both sites), K[83], and K[18] by ubiquitin site analysis using mass spectrometry, and a significantly higher level of K[66, 67]-ε-GG peptide was detected in HBB[1–cQ132] without lenalidomide treatment, compared to other conditions (**Extended Data Fig. 10c, Supplementary Information Table 6**). Although neither the HBB[1–cQ132] nor recombinant HBB was amenable to electroporation, which precluded our ability to evaluate CRBN-dependent degradation in cells, these data demonstrate that when the C-terminal cyclic imide modification is formed adventitiously on a protein like HBB[1–cQ132], the modification promotes CRBN-dependent ubiquitination of the protein.

To investigate whether the level of C-terminal cyclic imides across proteins is dependent on the availability of the thalidomide-binding domain of CRBN in cells, we performed a quantitative proteomics experiment to compare the global proteome obtained from HEK293T cells before and after CRBN knockout by CRISPR/Cas9 or treatment with lenalidomide using exogenously added GFP as an internal control. We found 39 unique peptides bearing C-terminal cyclic imides and observed most of these modified peptides increase when CRBN is knocked out or the thalidomide-binding domain of CRBN is inhibited by lenalidomide (**Fig. 5c, Extended Data Fig. 10d, Supplementary Information Table 7**). A similar increase in 34 out of 36 peptides bearing a C-terminal cyclic imide was identified in MM.1S cells after treatment with lenalidomide (**Fig. 5d, Supplementary Information Table 7**). Importantly, peptides bearing C-terminal asparagine and glutamine also increase in both cell lines upon CRBN knockout or inhibition, consistent with a model where blockade of degradation of substrates bearing the C-terminal imide allows the modifications to be hydrolyzed (**Extended Data Fig. 10e–f, Supplementary Information Table 7**).

We selected ACTB cN111 for closer evaluation to more sensitively detect and quantify these changes (highlighted in blue, **Fig. 4c**). SIM quantification of ACTB cN111 and N111 from HEK293T or MM.1S cell lysates spiked with heavy ACTB peptides (ACTB[96*–113], ACTB[96*–cN111], ACTB[96*–N111]) as an internal standard showed a 25–36% and 76–77% increase in the modifications relative to the parent peptide after 48 h treatment with lenalidomide (**Fig. 5e–f**, **Extended Data Fig. 10g**). Thus, the thalidomide-binding domain of CRBN appears to

promote the ubiquitination and eventual degradation of endogenous substrates bearing the C-terminal cyclic imide degron, which form in a surprisingly rapid manner to prevent the unwanted accumulation of these fragments and their hydrolysis products over time.

Discussion

We utilized a targeted protein degradation strategy to discover that previously underappreciated C-terminal cyclic imide modifications possess properties that are prototypical for a degron and are physiologically recognized on endogenous substrates by the thalidomide-binding domain of CRBN. Observation of the C-terminal cyclic imide modification on thousands of sites across the proteome indicates that these modifications may represent an overlooked form of protein damage that is generated adventitiously at susceptible asparagine and glutamine residues. A model for the C-terminal cyclic imide modification as a form of protein damage is reminiscent of another form of spontaneous protein damage, the isoaspartate PTM, which arises from spontaneous deamidation at asparagine, and conservation of the cellular machinery (*e.g.*, PIMT) to protect organisms from this form of protein damage is particularly important in the brain.[48] Likewise, loss of the thalidomide-binding domain of CRBN is associated with intellectual disability.[12] The deleterious effects of this form of protein damage may therefore be most pronounced in vivo, where C-terminal cyclic imide-bearing proteins, and particularly their downstream hydrolyzed products, may accumulate to a greater degree. Whether the hydrolyzed products are removed separately if they are not intercepted by CRBN is an open question. Although CRBN likely has additional endogenous substrates and functions, these observations are congruent with a model where CRBN is conserved to regulate the removal of the C-terminal cyclic imide, thus preventing the deleterious accumulation of protein fragments.

Future studies on the genesis of C-terminal cyclic imides and comparison to the IMiDs will enable a stronger definition of the physiological function of CRBN, and may lead to the identification of biomarkers, rationalization of clinical effects, or discovery of novel induced substrates that are impacted by ligand engagement of CRBN. For example, the contribution of the epimers of the C-terminal cyclic imide to the biological function of the degron and the physiological role of CRBN, in comparison to the separate enantiomers of the IMiDs, is an area of future evaluation. In addition to a spontaneous internal cyclization mechanism, C-terminal cyclic imide modifications may form by other enzymatic means, as intriguingly several reported substrates of CRBN have protein termini that end in N or Q residues and our analysis of large proteomics datasets shows many instances of C-terminal cyclic imides found at the naturally occurring C-termini of proteins. Evaluation of the role of the cyclic imide PTM will be accelerated by the development of specific enrichment and detection methods for C-terminal cyclic imides to visualize and map these PTMs. As C-terminal cyclic imide sites and substrates become more clearly defined, further studies will elucidate the implications of these PTMs and their role in protein regulation and cellular signaling with respect to mechanisms regulated by CRBN and beyond.

References and Notes

1 Ito, T. *et al. Science* **327**, 1345-1350 (2010).
2 Krönke, J. *et al. Science* **343**, 301-305 (2014).
3 Lu, G. *et al. Science* **343**, 305-309 (2014).
4 Kronke, J. *et al. Nature* **523**, 183-188 (2015).

5 Winter, G. E. *et al. Science* **348**, 1376-1381 (2015).
6 Lu, J. *et al. Chem Biol* **22**, 755-763 (2015).
7 Nowak, R. P. *et al. Nat Chem Biol* **14**, 706-714 (2018).
8 Donovan, K. A. *et al. eLife* **7**, e38430 (2018).
9 Matyskiela, M. E. *et al. Nat Chem Biol* **14**, 981-987 (2018).
10 Asatsuma-Okumura, T. *et al. Nat Chem Biol* **15**, 1077-1084 (2019).
11 Lupas, A. N., Zhu, H. & Korycinski, M. *PLoS Comput Biol* **11**, e1004023 (2015).
12 Higgins, J. J., Pucilowska, J., Lombardi, R. Q. & Rooney, J. P. *Neurology* **63**, 1927-1931 (2004).
13 Bachmair, A., Finley, D. & Varshavsky, A. *Science* **234**, 179-186 (1986).
14 Koren, I. *et al. Cell* **173**, 1622-1635 e1614 (2018).
15 Maxwell, P. H. *et al. Nature* **399**, 271-275 (1999).
16 Gray, W. M., Kepinski, S., Rouse, D., Leyser, O. & Estelle, M. *Nature* **414**, 271-276 (2001).
17 Fischer, E. S. *et al. Nature* **512**, 49-53 (2014).
18 Del Prete, D., Rice, R. C., Rajadhyaksha, A. M. & D'Adamio, L. *J Biol Chem* **291**, 17209-17227 (2016).
19 Chamberlain, P. P. *et al. Nat Struct Mol Biol* **21**, 803-809 (2014).
20 Hartmann, M. D. *et al. J Struct Biol* **188**, 225-232 (2014).
21 Boichenko, I., Deiss, S., Bar, K., Hartmann, M. D. & Hernandez Alvarez, B. *J Med Chem* **59**, 770-774 (2016).
22 Schilling, S. *et al. Nat Med* **14**, 1106-1111 (2008).
23 Geiger, T. & Clarke, S. *J Biol Chem* **262**, 785-794 (1987).
24 Voorter, C. E., de Haard-Hoekman, W. A., van den Oetelaar, P. J., Bloemendal, H. & de Jong, W. W. *J Biol Chem* **263**, 19020-19023 (1988).
25 Tyler-Cross, R. & Schirch, V. *J Biol Chem* **266**, 22549-22556 (1991).
26 Brennan, T. V. & Clarke, S. *Int J Pept Protein Res* **45**, 547-553 (1995).
27 Paulus, H. *Annu Rev Biochem* **69**, 447-496 (2000).
28 Mills, K. V., Manning, J. S., Garcia, A. M. & Wuerdeman, L. A. *J Biol Chem* **279**, 20685-20691 (2004).
29 Shah, N. H. & Muir, T. W. *Chem Sci* **5**, 446-461 (2014).
30 Sakamoto, K. M. *et al. Proc Natl Acad Sci U S A* **98**, 8554-8559 (2001).
31 Nguyen, T. V. *et al. Mol Cell* **61**, 809-820 (2016).
32 Smith, B. E. *et al. Nat Commun* **10**, 131 (2019).
33 Lin, Z. *et al. J Am Chem Soc* **144**, 606-614 (2022).
34 Sievers, Q. L. *et al. Science* **362**, eaat0572 (2018).
35 Li, M. *et al. J Am Chem Soc* **137**, 14084-14093 (2015).
36 Jiang, B. *et al. Angew Chem Int Ed Engl* **58**, 6321-6326 (2019).
37 Paulus, H. *Annual Review of Biochemistry* **69**, 447-496 (2000).
38 Zhang, B. *et al. Nature* **513**, 382-387 (2014).
39 Mertins, P. *et al. Nature* **534**, 55-62 (2016).
40 Chen, T. W. *et al. Nat Commun* **8**, 465 (2017).
41 Clark, D. J. *et al. J Proteome Res* **17**, 2205-2215 (2018).
42 Gao, Q. *et al. Cell* **179**, 561-577 e522 (2019).
43 Clark, D. J. *et al. Cell* **179**, 964-983 e931 (2019).
44 Wang, L. B. *et al. Cancer Cell* **39**, 509-528 (2021).
45 Bryk, A. H. & Wisniewski, J. R. *J Proteome Res* **16**, 2752-2761 (2017).
46 Takata, T., Oxford, J. T., Demeler, B. & Lampi, K. J. *Protein Sci* **17**, 1565-1575 (2008).

47 Wilmarth, P. A. *et al. J Proteome Res* **5**, 2554-2566 (2006).
48 Kim, E., Lowenson, J. D., MacLaren, D. C., Clarke, S. & Young, S. G. *Proc Natl Acad Sci U S A* **94**, 6132-6137 (1997).

Extended Data and **Supplementary Information** are available for this paper.

Acknowledgments: We thank Y. Amako, D. Miyamoto, and A. D'Souza for helpful discussions and S. Trager, B. Budnik, and R. Robinson from the Harvard University Mass Spectrometry and Proteomics Resource Laboratory, Z. Niziolek from the Harvard University Bauer Core for technical support, and the Agilent Center of Excellence in Biomolecular Characterization for instrumentation. His-CRBN/DDB1 was a generous gift from Bristol Myers Squibb. Some data used in this publication were generated by the Clinical Proteomic Tumor Analysis Consortium (NCI/NIH). Support from the Ono Pharma Foundation (C.M.W.), Sloan Research Foundation (C.M.W.), Camille–Dreyfus Foundation (C.M.W.), the Blavatnik Biomedical Accelerator at Harvard University (C.M.W), the National Institutes of Health (R01GM114537, M.R.P.), Japan Society for the Promotion of Science (S.I.), and National Science Foundation (H.A.F.) are gratefully acknowledged.

Author contributions: S.I., N.V., and D.S. designed and synthesized compounds. S.I. and W.X. designed and performed degradation assays. H.A.F., S.I., W.X., and H.C.L. designed and conducted studies on binary and ternary complex evaluations. H.A.F., H.C.L., and S.I. designed and performed the preparation of degron-bearing proteins and evaluation of the engineered proteins. W.X., H.A.F., and S.I. investigated the formation of cyclic imide PTMs, their destruction via hydrolysis, and their half-lives. W.X., H.A.F., and S.I. prepared samples for proteomics experiments. W.X. designed and performed proteomics experiments, and analyzed the proteomics data jointly with C.M.W. B.W. and M.R.P. performed expressed protein ligation. C.M.W. conceived of the project and drafted the manuscript. All authors reviewed and edited the manuscript.

Competing interests: Harvard University has filed a patent application (US Provisional Application No. 63/174,389, April 13, 2021) including work described herein. C.M.W., S.I., H.A.F., and W.X. are inventors of this patent. All other authors declare no competing interests.

Additional information: All data are available in the main text or the Supplementary Information. Proteomics data have been deposited to the PRIDE repository with the dataset identifiers PXD025413, PXD030091, and PXD034248. A provisional patent has been filed by Harvard University. The authors declare no other competing interests. Correspondence and requests for materials should be addressed to C.M.W. (cwoo@chemistry.harvard.edu).

Methods

***In vivo* degradation assay of substrates.** 1.5×10^6 HEK293T or Jurkat cells were seeded in DMEM or RPMI supplemented with 10% FBS and 1× penicillin-streptomycin and incubated at 37 °C, 5% CO_2 for 30 min, then treated with compounds of interest and incubated at 37 °C, 5% CO_2 for the indicated time prior to collection and lysis. If noted, cells were treated with 1 μM MLN4924 for 1 h before treatment with compounds following the initial 30 min incubation. All compounds were dissolved in DMSO, and the final DMSO concentration after addition of the compound to the cells did not exceed 0.2% (v/v).

AlphaScreen. AlphaScreen buffer (3× stock solution: 150 mM HEPES pH 7.4, 600 mM NaCl, 0.3% w/v BSA, 3 mM TCEP) was prepared fresh for each experiment. A 3× stock solution of each compound (60 μM, 3% DMSO final/1× AlphaScreen buffer) and a series of 2-fold serial dilutions, in 3% DMSO/1× AlphaScreen buffer, were prepared fresh for each experiment. A solution of 750 nM His_6-CRBN/DDB1, 375 nM GST-BRD4(BD2)/1× AlphaScreen buffer (5 μL) was added to each well of a 384-well Optiplate. Then, compound (5 μL) was added, with each concentration assayed in triplicate. As a positive control, 10 μL 100 nM GST-His_6 was added to three wells. The plate was sealed with TopSeal-A PLUS, centrifuged (200 × g, 25 °C, 1 min), and incubated at 25 °C for 1 h. Under low light, the seal was removed and 5 μL of 60 μg/mL AlphaScreen Glutathione Donor beads, 60 μg/mL AlphaLISA Nickel Chelate Donor beads/1× AlphaScreen buffer was added to each well. The plate was sealed with TopSeal-A PLUS, centrifuged (200 × g, 25 °C, 1 min), and incubated at 25 °C for 1 h. The seal was removed and the plate was analyzed. Prior to analysis, the plate reader was calibrated with a plate containing 15 μL of 20 μg/mL Omnibeads/1× AlphaScreen buffer in the corner wells. Analysis was performed in Graphpad Prism, using the vehicle-treated wells as the baseline, fitting the signal from each compound to a Gaussian curve, and calculating the area under the curve (AUC). AUC results from each plate were normalized to dBET6.

Immunoprecipitation with monovalent compounds. Samples were prepared in technical triplicate for each condition. HEK-CRBN cells (80% confluence, 10 cm dishes) were transiently transfected with pcDNA3.1-IKZF1-EPEA. The transfection mix, containing 10 μg plasmid, 1 mL Opti-MEM I reduced serum media, and 10 μL TransIT Pro, was incubated at 25 °C for 15 min prior to dropwise addition to the culture. Cells were harvested 48 h after transfection and lysed in 1× protease/phosphatase inhibitor/1× non-denaturing lysis buffer (500 μL) and clarified by centrifugation (21,000 × g, 4 °C, 10 min). Clarified lysate (250 μL) was incubated with 100× compound stock (2.5 μL, final concentration: 1 μM) or DMSO on a tube rotator at 4 °C for 2 h. The solution was collected and then incubated with anti-FLAG M2 magnetic beads on a tube rotator at 4 °C for 1 h. The magnetic beads were washed with 1% Triton-100 in TBS (6× 1 mL). The enriched proteins were eluted by the addition of 125 μL 5% SDS/50 mM TEAB and heated at 95 °C for 10 min, and the supernatant was kept for proteomics sample preparation.

Preparation of immunoprecipitated samples for quantitative proteomics. Immunoprecipitated samples were reduced by addition of dithiothreitol (20 mM) at 24 °C for 30 min then alkylated by addition of iodoacetamide (40 mM) and incubation in the dark at 24 °C for 30 min. The samples were desalted and digested using a S-Trap micro.[3,4] Samples were acidified by the addition of phosphoric acid to a final concentration of 1.2%. S-Trap buffer (90% methanol, 0.1 M TEAB, pH 7.1, 165 μL) was then added. Each sample was transferred to a S-Trap micro column. Using a vacuum manifold, the columns were washed with S-Trap buffer (3 × 150 μL). To digest the S-trap-bound proteins, 1 μg of trypsin resuspended in 25 μL 50 mM TEAB, pH 8.0 was added to each column and incubated at 47 °C for 2 h without rotation. The digested peptides were eluted by

sequential addition of 50 mM TEAB, pH 8.0 (40 µL), 0.2% formic acid (40 µL), and 0.2% formic acid, 50% acetonitrile/water (40 µL), with each elution collected by centrifugation (4,000 × g, 24 °C, 1 min) in a clean Eppendorf tube. The eluted samples were concentrated to dryness in a vacufuge and resuspended in 25 µL ddH_2O. For each resuspended sample, 10 µL was taken for labeling with TMTpro 16-plex reagent (10 µL, 3 replicates × 5 conditions = 15 channels used) at 24 °C for 1 h. Hydroxylamine (5%, 5 µL) was added to each sample to quench the TMT reagent, and the samples were incubated at 24 °C for 15 min. The TMT-labeled samples were combined and dried in a vacufuge. The dried sample was resuspended in 300 µL 0.1% trifluoroacetic acid (TFA) and fractionated to 5 fractions using a Pierce high pH reversed-phase peptide fractionation kit. The peptides were eluted sequentially by 5% acetonitrile/0.1% triethylamine (TEA), followed by 10%, 20%, 35% and 50% acetonitrile/0.1% TEA. The first fraction (5% acetonitrile/0.1% TEA) was excluded from LC-MS/MS analysis. The other 4 fractions were concentrated to dryness and each sample was resuspended in 20 µL of 0.1% formic acid prior to LC-MS/MS analysis.

Global quantitative proteomics sample preparation. Global proteomics samples were prepared in biological triplicate for each condition. 1.5×10^6 HEK293T or MM.1S cells were seeded in 6-well plates and incubated at 37 °C, 5% CO_2 for 30 min. Small molecules of interest were then added, and cells were incubated at 37 °C, 5% CO_2 for the indicated time. Cells were collected according to the described general procedure, lysed by probe sonication (5 sec on, 3 sec off, 15 sec in total, 11% amplitude) in lysis buffer (5% SDS in 50 mM triethylammonium bicarbonate (TEAB), pH 7.55), and cleared by centrifugation (21,000 × g, 4 °C, 10 min). After protein quantification by BCA protein assay, the lysates were diluted to 1 mg/mL with the lysis buffer. The diluted lysates (100 µL) were reduced by addition of dithiothreitol (20 mM) at 24 °C for 30 min then alkylated by addition of iodoacetamide (40 mM) and incubation in the dark at 24 °C for 30 min. The samples were desalted and digested using a S-Trap micro.[49,50] Samples were acidified by the addition of phosphoric acid to a final concentration of 1.2%. S-Trap buffer (90% methanol, 0.1 M TEAB, pH 7.1, 900 µL) was then added. Each sample was transferred to a S-Trap micro column. Using a vacuum manifold, the columns were washed with S-Trap buffer (3 × 150 µL). To digest the S-trap-bound proteins, 4 µg of trypsin/Lys-C mix resuspended in 40 µL 50 mM TEAB pH 8.0 was added to each column and incubated at 37 °C for 16 h without rotation. The digested peptides were eluted by sequential addition of 50 mM TEAB pH 8.0 (40 µL), ddH_2O (40 µL) and 0.2% formic acid, 50% acetonitrile/water (35 µL), with each elution collected by centrifugation (4,000 × g, 24 °C, 1 min) in a clean Eppendorf tube. The eluted samples were concentrated to dryness in a vacufuge and resuspended in ddH_2O. For each resuspended sample, 5 µL was taken for labeling with TMT reagent (2 µL) at 24 °C for 1 h such that the combined total protein was 100 µg. Hydroxylamine (50%, 1.2 µL) was added to each sample to quench the TMT reagent, and the samples were incubated at 24 °C for 15 min. The TMT-labeled samples were combined and dried in a vacufuge. The dried sample was resuspended in 300 µL 0.1% trifluoroacetic acid (TFA) and fractionated to 20 fractions using a Pierce high pH reversed-phase peptide fractionation kit. The peptides were eluted sequentially by 4% acetonitrile/0.1% triethylamine (TEA) through 20% acetonitrile/0.1% TEA in 1% acetonitrile increments (17 fractions), followed by 25%, 30% and 50% acetonitrile/0.1% TEA. The first fraction (4% acetonitrile/0.1% TEA) was excluded from LC-MS/MS analysis. The other fractions were concentrated to dryness and each sample was resuspended in 20 µL of 0.1% formic acid prior to LC-MS/MS analysis.

Proteomics mass spectrometry acquisition procedures for protein level quantitation. Desalted and fractionated samples were resuspended in 0.1% formic acid/water (20 µL per sample). The samples (10 µL) were loaded onto a C18 trap column (3 cm, 3 µm particle size C18 Dr. Maisch 150 µm I.D) and then separated on an analytical column (50 cm PharmaFluidics,

Belgum) at 0.2 μL/min with a Thermo Scientific Ultimate 3000 system connected in line to a Thermo Scientific Orbitrap Fusion Lumos Tribrid. The column oven temperature was maintained at 35 °C. Peptides were eluted using a multi-step gradient at a flow rate of 0.2 μL/min over 180 min (0−15 min, 2–10% acetonitrile in 0.1% formic acid/water; 15−150 min, 10−40%; 150−170 min, 40−95%; 170−180 min, 95%) for IP proteomics and 90 min (0−15 min, 7% acetonitrile in 0.1% formic acid/water; 15−65 min, 7−37%; 65−75 min, 37−95%; 75−85 min, 95%; 85−90 min, 95−2%) for global proteomics. The electrospray ionization voltage was set to 2.2 kV and the capillary temperature was set to 275 °C. Dynamic exclusion was enabled with a mass tolerance of 10 ppm and exclusion duration of 90 or 150 sec. MS1 scans were performed over 410–1800 m/z at resolution 120,000. HCD fragmentation was performed on the top ten most abundant precursors exhibiting charge states from two to five at a resolving power setting of 60,000 and fragmentation energy of 37 or 38% in the Orbitrap. CID fragmentation was applied with 35% collision energy, and resulting fragments were detected using the normal scan rate in the ion trap.

Mass spectrometry data analysis for protein level quantitation. Analysis was performed in Thermo Scientific Proteome Discoverer version 2.4.1.15. The raw data were searched against SwissProt human (*Homo sapiens*) protein database (19 August 2016; 20,156 total entries) and contaminant proteins using the Sequest HT algorithm. Searches were performed with the following guidelines: spectra with a signal-to-noise ratio greater than 1.5; mass tolerance of 10−20 ppm for the precursor ions and 0.02 Da (HCD) and 0.6 Da (CID) for fragment ions; full trypsin digestion; 2 missed cleavages; variable oxidation on methionine residues (+15.995 Da); static carboxyamidomethylation of cysteine residues (+57.021 Da); static TMT labeling (+226.163 Da for TMT 10-plex or +304.207 Da for TMTpro 16-plex) at lysine residues and N-termini. The TMT reporter ions were quantified using the Reporter Ions Quantifier node and normalized to the amount of CRBN for IP proteomics and total peptide amount for global proteomics. Peptide spectral matches (PSMs) were filtered using a 1% false discovery rate (FDR) using Percolator. PSMs were filtered to PSMs in only one protein group with an isolation interference under 70%. For the obtained proteome, the data were further filtered to include only master proteins with high protein FDR confidence and exclude all contaminant proteins. For IP proteomics, the ratios and p-values were obtained from Proteome Discoverer (p-values were calculated by one-way ANOVA with TukeyHSD post-hoc test). For global proteomics, the data were further processed according to the methods of Huber and coworkers.[51] The model incorporates dependence of the variance on the mean intensity and a variance-stabilizing data transformation. In brief, missing abundances were filled in with minimum noise level computed by taking the minimum for each channel in Control and minimum for each channel in Treatment. A set of 2000 centroids were generated at random from the absolute maximum in the Control and Treatment and the absolute minimum in Control and Treatment, and a minimum noise level was generated using a K-means clustering method. If one abundance was missing, then the instance was filled with the geometric mean of the PSM for Control or Treatment. If all abundances were missing for Control and Treatment or the variance between existing abundances was above 30%, the PSM was removed. P-values for the abundance ratios were calculated using the t-test (background) method. The code used for data analysis is available on GitHub:
https://github.com/harvardinformatics/quantproteomics/tree/master/PEA

Cell viability assay. 2.0×10^4 MM.1S cells were seeded in each well of a 96-well plate containing 100 μL RPMI supplemented with 10% FBS and 1× penicillin-streptomycin. The compound of interest was added to each well to a final concentration of 10 nM–100 μM from 100× stock solutions in 4% DMSO/PBS (1 μL). Samples were incubated at 37 °C, 5% CO_2 for 5 days. Each well was treated with 3-(4,5-Dimethylthiazol-2-yl)-2,5-diphenyltetrazolium (MTT, 4 mg/mL, 10

μL), and the treated plate was incubated at 37 °C, 5% CO_2 for 3 h. The formazan crystals were solubilized by the addition of 100 μL of 10% SDS, 0.01 M HCl per well, and the plate was allowed to incubate at 37 °C overnight. The absorbance at 570 nm was measured to quantify the formazan generated in each well. The blank was defined by wells containing media and MTT reagent without any cells. For each treatment well, the cell viability was calculated by subtracting the blank value and normalizing to the average absorbance of the vehicle control wells (cells treated with 4% DMSO/PBS only).

Protein overexpression and purification of SrtA and GFP-LPETG. The procedure for overexpression and purification of SrtA was adapted from Liu and co-workers and Zenobi-Wong and co-workers.[52,53] BL21 (DE3) cells transformed with pET29-eSrtA were used to inoculate overnight cultures of LB + 50 μg/mL kanamycin, which were then incubated at 37 °C with shaking at 200 rpm for approximately 16 h. For each large-scale overexpression, kanamycin was added to 750 mL autoclaved LB to a final concentration of 50 μg/mL and the culture was inoculated with overnight culture diluted 1:100. The overexpression cultures were incubated at 37 °C with shaking at 200 rpm until the OD600 was approximately 0.5–0.8, at which point IPTG was added to a final concentration of 0.1 mM and the temperature was reduced to 30 °C. The cultures were incubated for 3 h prior to collecting the cells by centrifugation, flash freezing with liquid nitrogen, and storing at –80 °C. Up to 2 pellets, each from a 750 mL overexpression, were purified simultaneously. To purify protein, cell pellets were thawed on ice or in cool water, then resuspended in 10 mL of 0.1 mg/mL lysozyme, 1:1000 benzonase, 6 mM $MgCl_2$/B-PER per pellet. Lysates were incubated at 25 °C with shaking for 15 min, then were clarified by centrifugation (15,000 × g, 4 °C, 10 min), and syringe filtration (0.45 μm). The His-tagged protein was crudely purified on a Ni-bound 1 mL HiTrap Chelating HP column using standard methods, equilibrating and washing with 25 mM imidazole/PBS and eluting with a gradient to 500 mM imidazole/PBS. Protein-containing fractions, as determined by A280, not eluting with the dead volume were concentrated to approximately 1 mL and further purified on a S75 10/300 GL column, pre-equilibrated and run with TBS. Protein-containing fractions not eluting with the dead volume were collected and concentrated to approximately 100 μM with a 10 kDa MWCO spin concentrator, with protein concentration determined by measuring the A280 (ε = 14,440 M^{-1} cm^{-1}). The protein was aliquoted, flash frozen with liquid nitrogen, and stored at –80 °C.

The protocol for overexpression and purification of GFP-LPETG was adapted from Liu and coworkers.[35] pET28a-GFP-LPETG was constructed by adding the sequence encoding TGGSLPETG-His_6 to the C-terminus of GFP in pET28a:GFP. BL21 (DE3) cells transformed with pET28a-GFP-LPETG and were used to inoculate overnight cultures of LB + 50 μg/mL kanamycin, which were then incubated at 37 °C with shaking at 200 rpm for approximately 16 h. For each large-scale overexpression, kanamycin was added to 750 mL autoclaved LB to a final concentration of 50 μg/mL and the large-scale overexpression cultures were inoculated with overnight culture diluted 1:100. The overexpression cultures were incubated at 37 °C with shaking at 200 rpm until the OD600 was approximately 1, at which point IPTG was added to a final concentration of 0.45 mM and the temperature was reduced to 20 °C. The cultures were incubated for approximately 16 h prior to collecting the cells by centrifugation, flash freezing with liquid nitrogen, and storing at –80 °C. Up to 3 pellets, each from a 750 mL overexpression, were purified simultaneously. To purify protein, cell pellets were thawed on ice or in cool water, then resuspended in 8.3 mL of 25 mM imidazole, 1× protease inhibitor, 1% Triton-X 100/PBS per pellet. Lysates were combined and sonicated (30 sec on, 10 sec off, 5 min total, 25% amplitude) on ice. Lysates were clarified by centrifugation (20,000 × g, 4 °C, 10 min) and syringe filtration (0.45 μm). The His-tagged protein was crudely purified on a Ni-bound 1 mL HiTrap Chelating HP

column using standard methods, equilibrating and washing with 25 mM imidazole/PBS and eluting with a gradient to 500 mM imidazole/PBS. Protein-containing fractions, as determined by A280, were concentrated to approximately 1 mL and further purified on a S75 10/300 GL column, pre-equilibrated and run with TBS. Protein-containing fractions not eluting with the dead volume were collected and concentrated to approximately 200 μM with a 10 kDa MWCO spin filter, then diluted to 50 μM with TBS, with protein concentration determined by measuring the A488 (ε = 55,000 M^{-1} cm^{-1}). The protein was aliquoted, flash frozen with liquid nitrogen, and stored at –80 °C.

Sortase reaction. Conditions for the sortase reaction were adapted from Liu and coworkers and Ploegh and coworkers.[35,54] For each reaction, 10 μL of 50 μM GFP-LPETG or 100 μM GST-FKBP12-LPETG was combined with 2 μL of 10 mM peptide substrate in 37 μM of 100 mM Tris pH 7.5, 150 mM NaCl, 5 mM $CaCl_2$. Then, 1 μL of 97 μM eSrtA was added and the reaction was mixed by flicking. The reaction was allowed to incubate at 25 °C for 1 h. Non-reacted GFP-LPETG and eSrtA was removed by adding 25 μL of washed His-purification Dynabeads and incubating with inversion for 15 min. The supernatant was collected using a magnetic tube rack. To remove excess peptide substrate, a 0.5 mL Zeba 7 kDa desalting column was equilibrated three times with 300 μL of experiment buffer (centrifuging 1,500 × g, 25 °C, 1 min for each equilibration). The sample was added to the equilibrated column, which was centrifuged (1500 × g, 25 °C, 2 min). The flowthrough was collected. The final concentration of GFP was determined by measuring the A488 (ε = 55,000 M^{-1} cm^{-1}). For in cellulo experiments, the reaction was performed on a larger scale, with the volume of Dynabeads reduced to be equal to the volume of 50 μM GFP-LPETG or 100 μM GST-FKBP12-LPETG used. The larger-scale reactions were desalted using a 5 mL Zeba 7 kDa spin desalting column then concentrated using a 3 or 10 kDa MWCO spin concentrator. If not used immediately, proteins were flash frozen with liquid nitrogen and stored at –80 °C until use.

In vitro ubiquitination of C-terminally-tagged proteins or HBB[1–cQ132] and HBB[1–Me132]. 5.0×10^6 HEK-CRBN cells were collected per pellet, flash-frozen with liquid nitrogen, and stored at –80 °C until use. Approximately 1 pellet per 1.5 samples was thawed on ice, and each pellet was resuspended in 1x protease inhibitor cocktail/Pierce IP lysis buffer (250 μL). Lysates were incubated on ice for 10 min, then were clarified by centrifugation (21,000 × g, 4 °C, 10 min). The soluble portions of the lysates were collected, with 1 mL lysate per tube, and 150 μL of TBS-washed anti-FLAG M2 beads were added. Samples were incubated at 4 °C on a roller for 1 h. Using a magnetic tube rack, the beads were collected and washed 3× with 1 mL TBS. Each sample was then eluted by adding 100 μL of 100 ng/μL 3× FLAG peptide/TBS and incubating at 4 °C on a roller for 1 h. The eluent was collected. Substrate proteins were diluted to 5–7.5 μM in PBS, using the same protein concentration for all samples in each experiment, and 25× stocks of small molecules were prepared in 2.5% DMSO/PBS. Ubiquitination master mixes were prepared at 2× with and without E1 and E2 enzymes. Final concentrations (1×) of the master mix components were 0.2 μM UBE1, 2 μM UbcH5a, 1 mM UbcH5c, 400 μg/mL K0 ubiquitin, 1 μM ubiquitin aldehyde, 1× Mg-ATP, 1× E3 ligase buffer, 10 μM MG132, 100 nM MG101. Reactions were prepared by combining 6.25 μL FLAG eluent, 5.25 μL of target protein (6.25 μL if no small-molecule competition was performed in the experiment), 1 μL of 25× small molecule stock in 2.5% DMSO/PBS (final concentration: 100 μM), and 12.5 μL of ubiquitination master mix in PCR tubes. Reactions were incubated at 30 °C for 90 min then were stopped by the addition of 6.25 μL of 5× SDS-PAGE loading buffer. Samples were heated at 95 °C for 5 min prior to analysis by SDS-PAGE and western blotting.

Cellular degradation of C-terminally-tagged proteins. Cells were grown to 80–90% confluency in FBS-supplemented media without antibiotics (+/-) prior to electroporation. Cells were detached by trypsinization as necessary and washed with PBS, then resuspended in PBS and counted. For each sample, an equal number of cells (7×10^5–2.5×10^6) were aliquoted into a 1.7 mL tube and pelleted. Electroporation mixes were prepared for each sample type. Electroporation mixes for 100 µL tips were prepared by combining 311 µL Neon buffer R with 3.6 µL DMSO or 100× compound or, for experiments without small molecule competition, 315 µL Neon buffer R and 45 µL of 50–60 µM protein in PBS or TBS, using the same protein concentration for all samples in each experiment, or buffer alone for control samples. All protein concentrations were determined by nanodrop, using the same extinction coefficient for all proteins of the same type. Electroporation mixes for 10 µL tips were prepared for each sample type by combining 43.25 µL Neon buffer R with 0.5 µL DMSO or 100× compound and 6.25 µL of 50 µM protein in PBS, or TBS for control samples. Immediately prior to each electroporation, the PBS was removed from the pelleted cells and the pellet was resuspended in 110 µL or 12 µL of electroporation mix (for 100 and 10 µL tips, respectively). The sample was taken up into a tip attached to a Neon pipette, and the pipette tip was submerged in a Neon cuvette containing 3 mL Neon buffer E2. The sample was then electroporated (HEK293T cells 800 V, 25 msec, 2 pulses; Jurkat cells 1325 V, 10 msec, 3 pulses; MEF cells 1350 V, 30 msec, 1 pulse). The cells were then dispensed into 10 volumes of warmed PBS. This process was repeated for each sample, with each tip used for 3 electroporation cycles. Cells were then pelleted by centrifugation and the supernatant was removed. Cells were resuspended in 0.5 mL or 50 µL trypsin-EDTA solution (for 100 and 10 µL tips, respectively) and incubated at 37 °C for 5 min. Trypsinization was quenched by the addition of 0.5 mL DMEM +/− with DMSO or 1000× compound stock added to the media and cells electroporated with 100 µL tips were again pelleted. The supernatant was removed. Each sample was resuspended in 1 mL DMEM +/− and transferred to a well of a 12-well plate, with DMSO or 1000× compound stock added to the media. Cells electroporated with 10 µL tips were transferred directly to a 24-well plate. The samples were then incubated at 37 °C, 5% CO_2 until 6 h after electroporation. Cells were detached by trypsinization, agitation, and/or scraping, collected by centrifugation, and washed with PBS.

For analysis of GFP levels, each sample was resuspended in 500 µL PBS with 50 nM SYTOX Blue or 10 µL 0.5 mg/mL propidium iodide added to allow for exclusion of dead cells. Cells were analyzed by flow cytometry (mCherry, Pacific Blue, and FITC on LSRII or dsRed and FITC on Fortessa). At least 9,600 events were analyzed for each sample. Relative GFP level was determined by subtracting the arithmetic mean GFP signal among live cells in the control sample from the arithmetic mean GFP signal among live cells for each sample, then normalizing the resulting values to the arithmetic mean for GFP-His_6 or GFP-Me. For FKBP12 samples, cells were collected by centrifugation 6 h after electroporation and were lysed in 1% SDS, 1× protease inhibitor/PBS by brief electroporation (5 sec, 10% amplitude). Protein concentration was normalized by BCA assay, and samples were analyzed by Western blotting.

Proteomics for cyclic imide detection in red blood cells and bovine lens. Red blood cell samples were prepared in biological triplicate or quintuplicate, and bovine lens samples were prepared in quadruplicate for each condition. For trypsin digestion, lysates (100 µg per sample) were loaded on an S-trap micro column similarly as "Global Quantitative Proteomics Sample Preparation". To digest the S-trap-bound proteins, 2 µg of trypsin in 40 µL 50 mM TEAB, pH 7.4 was added to each column and incubated at 47 °C for 1 h without rotation. For chymotrypsin digestion, lysates were diluted to 1 mg/mL by 5% SDS, 50 mM TEAB, pH 7.55 and 100 µL of the lysates were taken to reduction and alkylation. The proteins were precipitated using methanol-chloroform

precipitation. In brief, four volumes of chilled methanol, one volume of chloroform and three volumes of water were added sequentially to the lysates. The mixture was vortexed and centrifugated at 14,000 × g, 5 min, 4 °C, and the supernatant aspirated. The protein pellet was washed with three volumes of methanol and centrifugated at 14,000 × g, 5 min, 4 °C, and the resulting precipitated protein was air-dried. The protein was dissolved in 200 µL 50 mM HEPES, 10 mM $CaCl_2$, pH 7.5, followed by the addition of 2.5 µg of chymotrypsin in 5 µL of 1 mM HCl. The digestion was allowed to proceed at 25 °C for 18 h without rotation and quenched by the addition of 10 µL of 10% FA. For both tryptic and chymotryptic peptides, approximately 40 µg of peptides in 10 µL ddH_2O per condition was taken for labeling with TMT reagent (10 µL) at 24 °C for 1 h. TMT labeling was quenched by 1M Tris-Cl (5 µL, pH 7.6) instead of hydroxylamine to minimize the hydrolysis of cyclic imides. For base ablation of the cyclic imides, the dried, digested samples were incubated with 1% triethylamine/H_2O (100 µL, pH 12.0) at 65 °C for 30 min. The base-treated samples were concentrated to dryness before TMT labeling. The combined sample after TMT labeling was resuspended in 0.1% TFA and 300 µL of solution containing approximately 100 µg peptides was taken to fractionation into 6 fractions at 5%, 10%, 15%, 20%, 25%, 35% and 50% acetonitrile/0.1% TEA using the Pierce high pH reversed-phase peptide fractionation kit. The first fraction (5% acetonitrile/0.1% TEA) was excluded from LC-MS/MS analysis. Immediately after the elution, each fraction was acidified by the addition of 5 µL of 10% formic acid. The fractions were concentrated to dryness and each sample was resuspended in 20 µL of 0.1% formic acid prior to LC-MS/MS analysis. Samples for cyclic imide detection were dried in a vacufuge set at 24 °C and the dried samples were stored at −20 °C or −80 °C to avoid long exposure to higher temperature.

Time-course study of formation of cyclic imide and its hydrolysis products. The synthetic peptides (20 µL, 5 mM stock in ddH_2O) were incubated in 20 mM ammonium acetate buffer (380 µL) at pH 7.4, 8.0, or 9.0 (final concentration: 250 µM). Samples were incubated in a sand bath pre-heated to 37 °C, and 30 µL was taken from each sample at t = 0 h (collected immediately after resuspension in pH 7.4 buffer), 24 h, 48 h, 72 h, 96 h, 120 h, 144 h, 168 h, 192 h and 240 h. Immediately after collection, the samples were quenched by the addition of 0.75 µL of 10% formic acid and stored at –80 °C until analysis. The MS samples were prepared by mixing 2 µL of the peptides, 18 µL 0.1% formic acid, and 20 µL acetonitrile. Peptides were injected on a Thermo Orbitrap Fusion Lumos Tribrid or LTQ Orbitrap Velos and eluted using a multi-step gradient at a flow rate of 0.2 µL/min over 60 min (0−5 min, 5% acetonitrile in 0.1% formic acid/water; 5−52 min, 5−80%; 52−55 min, 80−98%; 55−60 min, 98%). The electrospray ionization voltage was set to 2 kV and the capillary temperature was set to 275 °C. MS1 scans were performed over 400–2000 m/z at resolution of 120,000. The raw chromatograms were extracted with m/z of label-free parent peptide (1030.47–1030.49), cyclic imide (908.39–908.41), and hydrolysis products (917.39–917.41) for HBB[42−60]; parent peptide (978.03–978.05), cyclic imide (856.46–856.48), and hydrolysis products (865.46–865.48) for ACTB[96−113]; parent peptide (999.83–999.85), cyclic imide (867.90–867.92 or 685.34–685.36), and hydrolysis products (876.90–876.92 or 703.35–703.37) for HBA[63−91]. For each species, only the peak area at the expected retention time was integrated and quantified using Genesis peak integration algorithm on Xcalibur Qual Browser. The quantification was performed as following: the mixture of HBB* (206.29 ng) was run on the full scan mode first (1) to obtain the absolute mass of unmodified parent peptide in the mixture. Then, HBB* was run alone on SIM mode to quantify the modified species (2) and lastly, the RBC digests spiked with HBB* mixture were run on the same SIM method to quantify the modified species in the RBC (3). The mass of HBB* injected was the same across all samples.

$$\%(mod/parent) = \frac{Area(light\ mod3)}{Area(heavy\ mod3)} \div \frac{Area(light\ parent3)}{Area(heavy\ parent3)} \times 100\%$$

$$Mass(mod) = 206.29\ ng \times \frac{Area(parent1)}{Area(TIC1)} \times \frac{Area(heavy\ mod2)}{Area(heavy\ parent2)} \times \frac{Area(light\ mod3)}{Area(heavy\ mod3)}$$

$$mod = cN\ or\ N\ peptide\ in\ the\ sample$$

Selected ion monitoring quantification of HBB parent and modified peptides in red blood cells. Red blood cell lysates (100 µg) were taken for reduction, alkylation and trypsin digestion as described in "Proteomics for Cyclic Imide Identification in Red Blood Cells and Bovine Lens". The peptides were desalted by Pierce peptide desalting spin columns and exactly following the manufacturer protocol. The dried samples were resuspended in 30 µL 0.1% FA. The isotopically labeled HBB[42*−60] (HBB*) was incubated in ammonium acetate buffer at pH 7.4, 37 °C for 48 h to generate the cyclic imide and hydrolysis products (final concentration: 250 µM). The MS samples were prepared by mixing 1 µL of the HBB* mixture, 10 µL of RBC digests, and 9 µL 0.1% FA. The sample (8 µL) was injected on a Thermo Orbitrap Fusion Lumos Tribrid and eluted using a multi-step gradient at a flow rate of 0.2 µL/min over 60 min (0−5 min, 5% acetonitrile in 0.1% formic acid/water; 5−52 min, 5−80%; 52−55 min, 80−98%; 55−60 min, 98%). The electrospray ionization voltage was set to 2 kV and the capillary temperature was set to 275 °C. MS1 scans were performed on the selected ion monitoring (SIM) mode to only look for m/z of 1029.88−1037.08, 908.30−915.50 and 917.31−924.51, and retention time window of 25−33 min, 33.5−50 min, and 33.5−50 min for the parent peptide, cyclic imide and hydrolyzed products, respectively. Orbitrap resolution was set at 120,000, RF lens at 60%, maximum injection time at 300 ms and normalized AGC target at 2000%. The raw chromatograms were extracted with m/z of light parent peptide (1030.47–1030.49), cyclic imide (908.39–908.41), and hydrolysis products (917.39–917.41) for RBC lysates and heavy parent peptide (1035.48–1035.50), cyclic imide (913.40–913.42), and hydrolysis products (922.40–922.42) for peptide standard. For each species, only the peak area with the expected retention time and isotope patterns was integrated and quantified using the ICIS peak integration algorithm on Xcalibur Qual Browser. The calculations for quantification can be found in Supplementary Information.

Generation of recombinant HBB[1–129] thioester. Constructs for *E. coli* expression were derived from the plasmid pcDNA3.1-HBB-FLAG and pTXB1-HSP27-AvaE-His_6. Inserts corresponding to HBB[1–129] and backbone excluding HSP27 were amplified using overhang PCR with primers designed for Gibson Assembly using NEBuilder online tools. The inserts were then ligated with pTXB1-AvaE-His_6 linear vector to generate recombinant plasmids using HiFi DNA Assembly Kit (NEB). Ligated DNAs were transformed into high efficiency DH5α competent cells (NEB) and the sequences validated by Sanger sequencing.

BL21(DE3) cells were transformed with the HBB[1–129]-AvaE-His_6 plasmid. A starter culture was grown overnight at 37 °C for 16 h from a single colony. Terrific Broth (3 mL, IBI Scientific) was then inoculated with the starter culture and grown to an OD600 of 0.6–0.8 at 37 °C while being shaken at 225 rpm. Expression was induced with IPTG at a final concentration of 1 mM followed by incubation at room temperature for 16 h with shaking at 225 rpm. Cells were then harvested at 6,000 × g, and the resulting pellets were resuspended in lysis buffer (20 mM NaH_2PO_4, 500 mM NaCl, 1 mM TCEP, 5 mM imidazole, and 2 mM phenylmethylsulfonyl fluoride, pH 7.0). Solid guanidine HCl was added to the slurry and the resulting were subjected to tip sonication on ice (30 sec on, 30 sec off, 5 min total, 70% amplitude) to break the protein inclusion-bodies. After clarification by centrifugation (20,000 × g, 4 °C, 30 min), the pH of lysate was adjusted to 6.8 with

3 M NaOH. The resulting supernatants were then loaded onto Cobalt-NTA agarose beads (Genessee Scientific), incubated at 4 °C for 1 h with slight agitation, and then extensively washed (4 M Urea, 20 mM NaH_2PO_4, 600 mM NaCl, 20 mM imidazole, pH 6.8) for 3 column volumes. The intein-fusion protein was then eluted (4 M Urea, 20 mM NaH_2PO_4, 600 mM NaCl, 1 mM TCEP, 250 mM imidazole, pH 6.8) and buffer exchange 500-fold into DPBS buffer with 4 M Urea by centrifugal filtering with 10K spin filters (Amicon Ultra, EMD Millipore) to remove excess imidazole. The intein fusion was then cleaved through transthioesterification by the addition of sodium mercaptoethanesulfonate (MESNa) to a final concentration of 250 mM at pH 6.8 prior to incubation at room temperature for 16 h. The cleaved AvaE-His_6 intein and unreacted fusion protein were removed by loading the mixture onto Co-NTA agarose beads, incubating at 4 °C for 3 h. The final protein thioester was obtained by elution with washing buffer (20 mM NaH_2PO_4, 600 mM NaCl, 20 mM imidazole, pH 6.8), followed by further purification by reversed-phase liquid chromatography. Pure protein was characterized by analytical C4 RP-HPLC and ESI-MS. Purified proteins were lyophilized prior to storage.

Ligation and deselenization for generation of HBB[1–cQ132] and HBB[1–Me132]. HBB[1–129] thioester (1.5 mg, 0.11 μmol, 1 mM final concentration, 1 eq.) and Sec-YcQ or Sec-YcQMe (0.2 mg, 0.36 μmol, 3 mM final concentration, 3 equiv.) were dissolved in 100 μL of degassed ligation buffer (6 M guanidine HCl, 100 mM phosphate, 100 mM L-ascorbic acid, 100 mM TCEP, 250 mM mercaptophenylacetic acid (MPAA), pH 7.0). The reaction was monitored by analytical C4 RP-HPLC and ligation was largely complete after 4 h at 25 °C with gentle agitation. The mixture was buffer exchanged 1000-fold into 6 M guanidine HCl, 100 mM phosphate pH 6.0 to remove MPAA using 3K centrifugal filters (Amicon Ultra, Millipore). Dithiothreitol (DTT) was added to a final concentration of 25 mM and the mixture was incubated for 10 min to fully reduce the selenocysteine residues. Solid TCEP was then added to a final concentration of 100 mM and the pH was adjusted to 5.0. Analytical RP-HPLC and ESI-MS were used to monitor the conversion of selenocysteine to alanine. After 2 h, deselenization was deemed complete, and the final product was purified by semipreparative RP-HPLC on a C4 column. The purity and identity of the product were confirmed by analytical RP-HPLC and qTOF-ESI-MS, respectively. HBB[1-cQ132] was found as an inseparable mixture consistent with the expected protein product and another product bearing a RtoG mutation due to misreading of the codon in E. *coli*, as has been observed previously.[14] Similarly, HBB[1-Me132] was found to have the same mixture, as well as the oxidation of two methionine residues.

Proteomics for cyclic imide detection in HEK293T and MM.1S cells. Samples were prepared in biological triplicate for each condition. 3×10^6 WT HEK293T cells or CRBN-KO HEK293T cells with the same passage number (p19) were collected in separate tubes. For lenalidomide treatment, 1.5×10^6 WT HEK293T cells (p19) were seeded in 6-well plates and incubated at 37 °C for 1 h. The cells were treated with 200 μM lenalidomide for 24 h first. Then, the media was aspirated and fresh media containing 200 μM lenalidomide was added into each well and incubated for another 24 h (48 h treatment in total). The procedure was the same for MM.1S cells, except that 2×10^6 cells were initially seeded and cells were spun down at 300 × g, 24 °C, 4 min and resuspended in fresh media containing lenalidomide after 24 h. After protein quantification by BCA assay, the lysates were diluted to 1 mg/mL with the lysis buffer. To the diluted lysate (100 μL), 0.5 μg of GFP-LPETG was added as an internal standard (0.42 μL of 43 μM TBS stock), and the mixtures were taken for reduction and alkylation. The samples were loaded on S-trap micro columns similarly as "Global Quantitative Proteomics Sample Preparation". To digest the S-trap–bound proteins, 2.5 μg of trypsin in 40 μL 50 mM TEAB pH 7.4 was added to each column and incubated at 47 °C for 1 h without rotation. TMT labeling was performed as described in

"Proteomics for Cyclic Imide Detection in Red Blood Cells and Bovine Lens". The combined sample after TMT labeling was resuspended in 900 µL 0.1% TFA and 300 µL was taken to fractionation into 18 fractions using the Pierce high pH reversed-phase peptide fractionation kit. The peptides were eluted sequentially by 5%, 6%, 8%, 10%, 11−20% (with 1% increments), 25%, 30%, 35% and 50% acetonitrile/0.1% TEA. Immediately after the elution, each fraction was acidified by the addition of 5 µL of 10% formic acid. The fractions were concentrated to dryness and each sample was resuspended in 20 µL of 0.1% formic acid prior to LC-MS/MS analysis.

Proteomics mass spectrometry acquisition procedures for cyclic imide detection. Desalted and fractionated samples were resuspended in 0.1% formic acid/water (20 µL per sample). The sample (2.0 µL) was loaded onto a C18 trap column (3 cm, 3 µm particle size C10 Dr. Maisch 150 µm I.D) and then separated on an analytical column (Thermo Scientific Acclaim PepMap 100, 2 µm particle size, 250 mm length, 75 µm internal diameter) at 0.2 µL/min with a Thermo Scientific Ultimate 3000 system connected in line to a Thermo Scientific Orbitrap Fusion Lumos Tribrid. The column temperature was maintained at 50 °C. Peptides were eluted using a multi-step gradient at a flow rate of 0.2 µL/min over 90 min (0−5 min, 2% acetonitrile in 0.1% formic acid/water; 5−7 min, 2−5%; 7−75 min, 5−40%; 75−85 min, 40−95%; 85−90 min, 95%) for HEK293T and MM.1S and 180 min (0−5 min, 2% acetonitrile in 0.1% formic acid/water; 5−15 min, 2-10%; 15−160 min, 10−40%; 160−170 min, 40−95%; 170−180 min, 95%) for RBC and bovine lens. The electrospray ionization voltage was set to 2 kV and the capillary temperature was set to 275 °C. Dynamic exclusion was enabled with a mass tolerance of 10 ppm and exclusion duration of 90 sec. MS1 scans were performed over 410–2000 m/z at resolution 120,000. HCD fragmentation was performed on the top ten most abundant precursors exhibiting a charge state from two to five at a resolving power setting of 60,000 and fragmentation energy of 37% in the Orbitrap. CID fragmentation was applied with 35% collision energy, and resulting fragments were detected using the normal scan rate in the ion trap.

Selected ion monitoring quantification of ACTB parent and modified peptides in HEK293T and MM.1S cells. Samples were prepared in biological quadruplicate for each condition. 1.5×10^6 WT HEK293T cells (p20) or 2×10^6 MM.1S cells (p14) were seeded in 6-well plates and incubated at 37 °C for 1 h. The cells were treated with DMSO or 200 µM lenalidomide for 24 h first. For HEK293T, the media was aspirated and fresh media containing 200 µM lenalidomide was added into each well and incubated for another 24 h. For MM.1S, the cells were centrifugated at 300 × g, 24 °C, 4 min and the media aspirated. Cells were reseeded in 6-well plates with fresh media containing DMSO or 200 µM lenalidomide and incubated for another 24 h (48 h treatment in total). Cells were reseeded in 6-well plates with fresh media containing DMSO or 200 µM lenalidomide and incubated for another 24 h (48 h treatment in total). Lysate preparation, reduction/alkylation, and trypsin digestion were performed as described in "Proteomics for Cyclic Imide Identification in HEK293T and MM.1S cells". The dried peptide digests (100 µg) were fractionated in to 8 fractions_using the Pierce high pH reversed-phase peptide fractionation kit. The peptides were eluted sequentially by 10%, 12%, 14%, 16%, 18%, 20%, 25% and 50% acetonitrile/0.1% TEA. Immediately after the elution, each fraction was acidified by the addition of 5 µL of 10% formic acid. The fractions were concentrated to dryness and each sample was resuspended in 20 µL of 0.1% formic acid. The isotopically labeled ACTB[96*−113] (ACTB*) was incubated in ammonium acetate buffer at pH 7.4, 37 °C for 48 h to generate the cyclic imide and hydrolysis products (final concentration: 250 µM). Each fraction was spiked with 0.75 µL of the ACTB[96*-113] incubation mixture. Samples were first run on the SIM mode on LTQ Orbitrap Velos in search of light ACTB peptides and modified species, which were found in fraction 12% for HEK293T and fractions 12% and 14% for MM.1S. The same fractionation procedure was performed on all

the samples. For HEK293T, fraction 12% was resuspended in 20 µL 0.1% FA + 0.75 µL ACTB* standard. For MM.1S, fractions 12% and 14% were dried and resuspended in 40 µL 0.1% FA + 1.5 µL ACTB* mixture in total. The sample (6 or 8 µL) was injected on a Thermo Orbitrap Fusion Lumos Tribrid and eluted using a multi-step gradient at a flow rate of 0.2 µL/min over 90 min (0−5 min, 5% acetonitrile in 0.1% formic acid/water; 5−65 min, 5−45%; 65−80 min, 45−98%; 80−90 min, 98%). The electrospray ionization voltage was set to 2 kV and the capillary temperature was set to 275 °C. MS1 scans were performed on SIM mode to only look for m/z of 977.44−982.64, 855.76−861.16 and 864.76−870.16, and retention time window of 25−40 min, 35−48 min, and 32−45 min for the parent peptide, cyclic imide and hydrolyzed products, respectively. Orbitrap resolution was set at 120,000, RF lens at 60%, maximum injection time at 300 ms and normalized AGC target at 2000%. The raw chromatograms were extracted with m/z of light parent peptide (978.03–978.05), cyclic imide (856.45–856.47), and hydrolysis products (865.45–865.47) for cell lysates and heavy parent peptide (981.03–981.05 for MM.1S and 981.04–981.06 for HEK293T), cyclic imide (859.45–859.47), and hydrolysis products (868.45–868.47 for MM.1S and 868.46–868.48 for HEK293T) for peptide standard. For each species, only the peak area with the expected retention time and isotope patterns was integrated and quantified using the ICIS peak integration algorithm on Xcalibur Qual Browser version 3.0.63. The quantification was performed as following: the mixture of ACTB* (91.89 ng) was run on the full scan mode first (1) to obtain the absolute mass of unmodified parent peptide in the mixture. Then, ACTB* was run alone on SIM mode to quantify the modified species (2) and lastly, the cell lysates spiked with ACTB* mixture were run on the same SIM method to quantify the modified species in the ACTB (3). For some samples of HEK293T, the mixture of ACTB* injected was 68.92 ng and the calculations of absolute masses were scaled accordingly (the ratios of modified species to parent peptide are unaffected). The p-values for the ratios were calculated by unpaired two-tailed t-tests.

$$\%(mod/parent) = \frac{Area(light\ mod3)}{Area(heavy\ mod3)} \div \frac{Area(light\ parent3)}{Area(heavy\ parent3)} \times 100\%$$

$$Mass(mod) = 91.89(68.92)\ ng \times \frac{Area(parent1)}{Area(TIC1)} \times \frac{Area(heavy\ mod2)}{Area(heavy\ parent2)} \times \frac{Area(light\ mod3)}{Area(heavy\ mod3)}$$

$$mod = cN\ or\ N\ peptide\ in\ the\ sample$$

Mass spectrometry data analysis for cyclic imide detection. Analysis was performed in Thermo Scientific Proteome Discoverer version 2.4.1.15. The raw data were searched against SwissProt human (*Homo sapiens*) protein database (21 February 2019; 20,355 total entries) or SwissProt bovine (*Bos taurus*) protein database (19 August 2016; 5,997 entries) and contaminant proteins using the Sequest HT algorithm. Searches were performed with the following guidelines: spectra with a signal-to-noise ratio greater than 1.5; mass tolerance of 20 ppm for the precursor ions and 0.02 Da (HCD) and 0.6 Da (CID) for fragment ions; semi-tryptic or semi-chymotryptic (FLWY) digestion with specificity at the peptide N-terminus only; 2 missed cleavages; variable oxidation on methionine residues (+15.995 Da); static carboxyamidomethylation of cysteine residues (+57.021 Da); static TMT labeling (+226.163 Da) at lysine residues and N-termini; variable dehydration on asparagine and glutamine residues at C-terminus only (–18.015 Da). The TMT reporter ions were quantified using the Reporter Ions Quantifier node and normalized to the intensity of GFP-LPETG peptides for HEK293T and MM.1S and the summed peptide intensity for RBC and bovine lens. Peptide spectral matches (PSMs) were filtered using a 1% or 5% FDR using Target Decoy PSM validator. For the obtained peptide groups, the data were further filtered to include only peptides with 1% or 5% FDR, bearing the modification of dehydration on

asparagine or glutamine residues, and derived from non-contaminant proteins to generate the list of peptides bearing C-terminal cyclic imide modifications. To generate the list of peptides bearing C-terminal glutamine or asparagine, the data were filtered to include only peptides with 1% or 5% FDR, bearing asparagine or glutamine residues at the peptide C-terminus, and derived from non-contaminant proteins. The peptides that were mapped back to the protein C-terminus were excluded. The p-values for the ratios were obtained by one-way ANOVA with TukeyHSD post-hoc test from Proteome Discoverer.

Identification of C-terminal cyclic imide modification sites from public datasets. Data were analyzed as described under "Mass spectrometry data analysis for cyclic imide detection" with the following modifications. For the analysis of global proteomics datasets obtained from CPTAC, the RAW datasets were processed according to the methods in the respective publication for fully tryptic peptides and spectra that did not receive a confident peptide spectral match were searched for N-terminal semi-tryptic sequences and an additional dynamic modification of dehydration on asparagine or glutamine residues (–18.015 Da) at the C-terminus of the peptide. The data were filtered with a 1% FDR using Percolator.

Additional References

49 Ludwig, K. R., Schroll, M. M. & Hummon, A. B. *J Proteome Res* **17**, 2480-2490 (2018).

50 HaileMariam, M. *et al. J Proteome Res* **17**, 2917-2924 (2018).

51 Huber, W., von Heydebreck, A., Sultmann, H., Poustka, A. & Vingron, M. *Bioinformatics* **18 Suppl 1**, S96-104 (2002).

52 Chen, I., Dorr, B. M. & Liu, D. R. *Proc Natl Acad Sci U S A* **108**, 11399-11404 (2011).

53 Broguiere, N., Formica, F. A., Barreto, G. & Zenobi-Wong, M. *Acta Biomater* **77**, 182-190 (2018).

54 Popp, M. W., Antos, J. M. & Ploegh, H. L. *Curr Protoc Protein Sci* **Chapter 15**, Unit 15 13 (2009).

55 Carbon, J. & Curry, J. B. *J Mol Biol* **38**, 201-216 (1968).

Figures

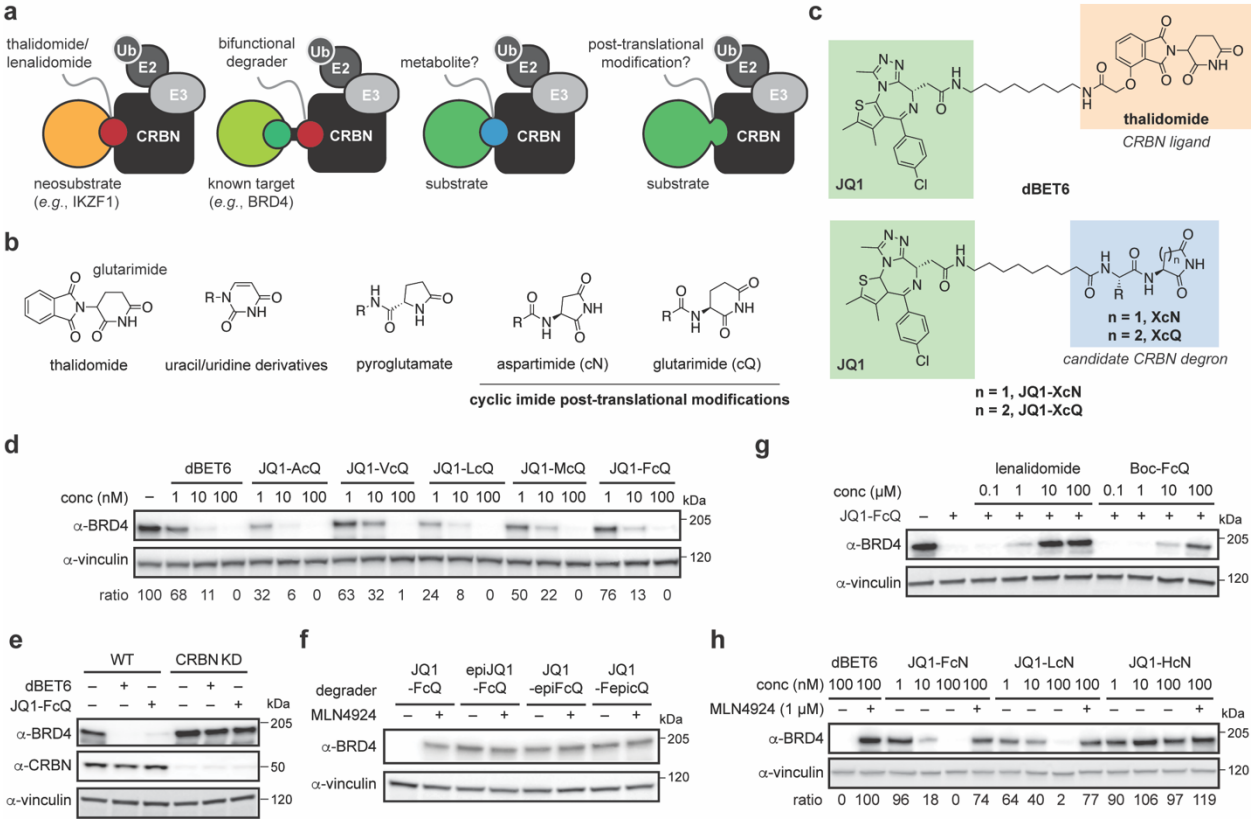

Fig. 1. Cyclic imide dipeptides functionally engage cereblon in targeted protein degradation. (**a**) CRBN is engaged by thalidomide and lenalidomide in a manner that may mimic the biological ligand. Models of CRBN engagement by either a small molecule or PTM-based degron. (**b**) Structure of thalidomide and candidate structures for the CRBN degron. (**c**) Structure of dBET6 and candidate dipeptide degraders JQ1-XcN and JQ1-XcQ for functional engagement of CRBN and target protein degradation in cells. (**d**) Western blot of BRD4 levels after treatment of HEK293T cells with the indicated glutarimide degrader over 1–100 nM. (**e**) Western blot of BRD4 after treatment of wild type (WT) or shRNA knockdown (CRBN KD) HEK293T cells with the indicated degrader. (**f**) Western blot of BRD4 after treatment of HEK293T cells with one of the three epimers of JQ1-FcQ at 100 nM. (**g**) Western blot of BRD4 after co-treatment of HEK293T cells with JQ1-FcQ and lenalidomide or Boc-FcQ. (**h**) Western blot of BRD4 levels after treatment of HEK293T cells with the indicated aspartimide degrader over 1–100 nM. All degradation assays were performed with 4 h incubation. All western blot data are representative of at least 2 independent replicates. For uncropped western blot images, see Supplementary Figure 6.

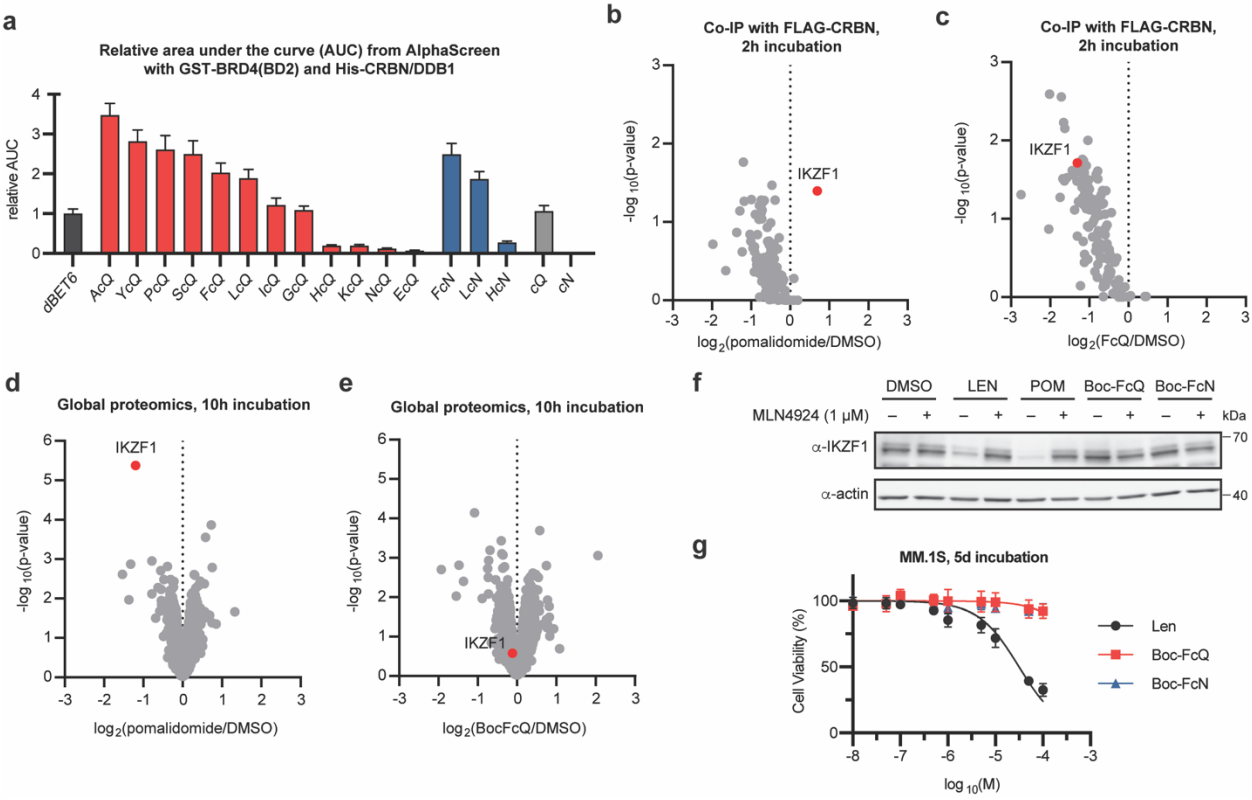

Fig. 2. Engagement of CRBN and ternary complex formation by dipeptide degraders, but not the dipeptides alone. (**a**) The relative area under the curve from AlphaScreen for ternary complex formation between GST-BRD4(BD2) and His-CRBN/DDB1 in the presence of the indicated degrader normalized to dBET6. AlphaScreen data is representative of 3 replicates. (**b–c**) Quantitative proteomics of co-immunoprecipitated proteins from lysates of HEK-CRBN cells overexpressing IKZF1 after 2 h incubation with 1 μM (**b**) pomalidomide or (**c**) FcQ. Protein levels were normalized to the amount of CRBN in each channel. (**d–e**) Quantitative proteomics of MM.1S cells after 10 h treatment with 10 μM (**d**) pomalidomide or (**e**) Boc-FcQ. (**f**) Western blot of IKZF1 levels after treatment with 10 μM of the indicated compound in MM.1S cells. Western blot data are representative of 3 independent replicates. (**g**) Cell viability (MTT) assay of the indicated compounds after treatment of MM.1S cells for 5 d. All proteomics experiments were performed in triplicates. For uncropped western blot images, see Supplementary Figure 7.

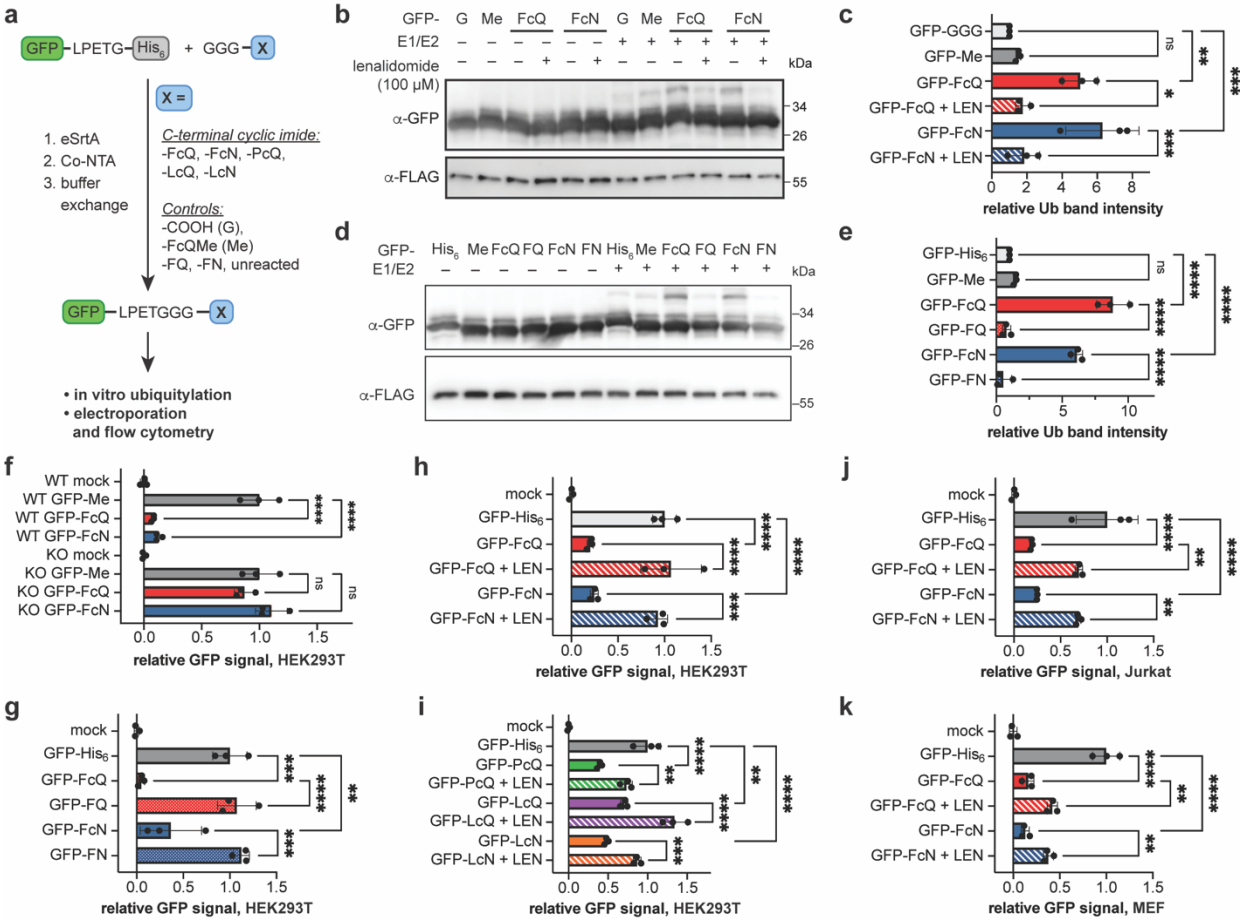

Fig. 3. C-Terminal cyclic imides are degrons that promote CRBN-dependent ubiquitination and degradation. (**a**) Sortase system used to generate degron-tagged GFP from GFP-LPETG-His_6. (**b**) In vitro ubiquitination of GFP tagged with C-terminal cyclic imide with K0 ubiquitin. GFP-G = GFP with C-terminal GGG; GFP-Me = GFP with C-terminal FcQMe; GFP-FcQ = GFP with C-terminal FcQ; GFP-FcN = GFP with C-terminal FcN. (**c**) Quantification of ubiquitinated protein band intensity in the experiment shown in (**b**) across three replicates. (**d**) In vitro ubiquitination of GFP tagged with uncyclized C-terminal glutamine or asparagine with K0 ubiquitin. (**e**) Quantification of ubiquitinated protein band intensity in experiment shown in (**d**) across three replicates. (**f**) Flow cytometry analysis of the GFP levels in WT or CRBN KO HEK293T cells 6 h after electroporation with GFP tagged with the indicated peptide. (**g**) Flow cytometry analysis of the GFP levels in HEK293T cells 6 h after electroporation with GFP tagged with the indicated peptide, with C-terminal Q and N cyclized or uncyclized. GFP-His_6 = GFP with C-terminal His_6 tag (no sortase treatment). (**h–i**) Flow cytometry analysis of the GFP levels in HEK293T cells 6 h after electroporation with GFP tagged with the indicated peptide, with or without lenalidomide competition (100 µM). (**j–k**) Flow cytometry analysis of the GFP levels in (**j**) Jurkat or (**k**) MEF cells 6 h after electroporation with GFP tagged with the indicated peptide, with or without lenalidomide competition (100 µM). Comparisons were performed using a one-way ANOVA with Šídák's multiple comparisons test. ns = not significant, * = $p < 0.05$, ** = $p < 0.01$, *** = $p < 0.001$, **** = $p < 0.0001$. All western blot and flow cytometry data are representative of three independent replicates. For uncropped western blot images, see Supplementary Figure 7.

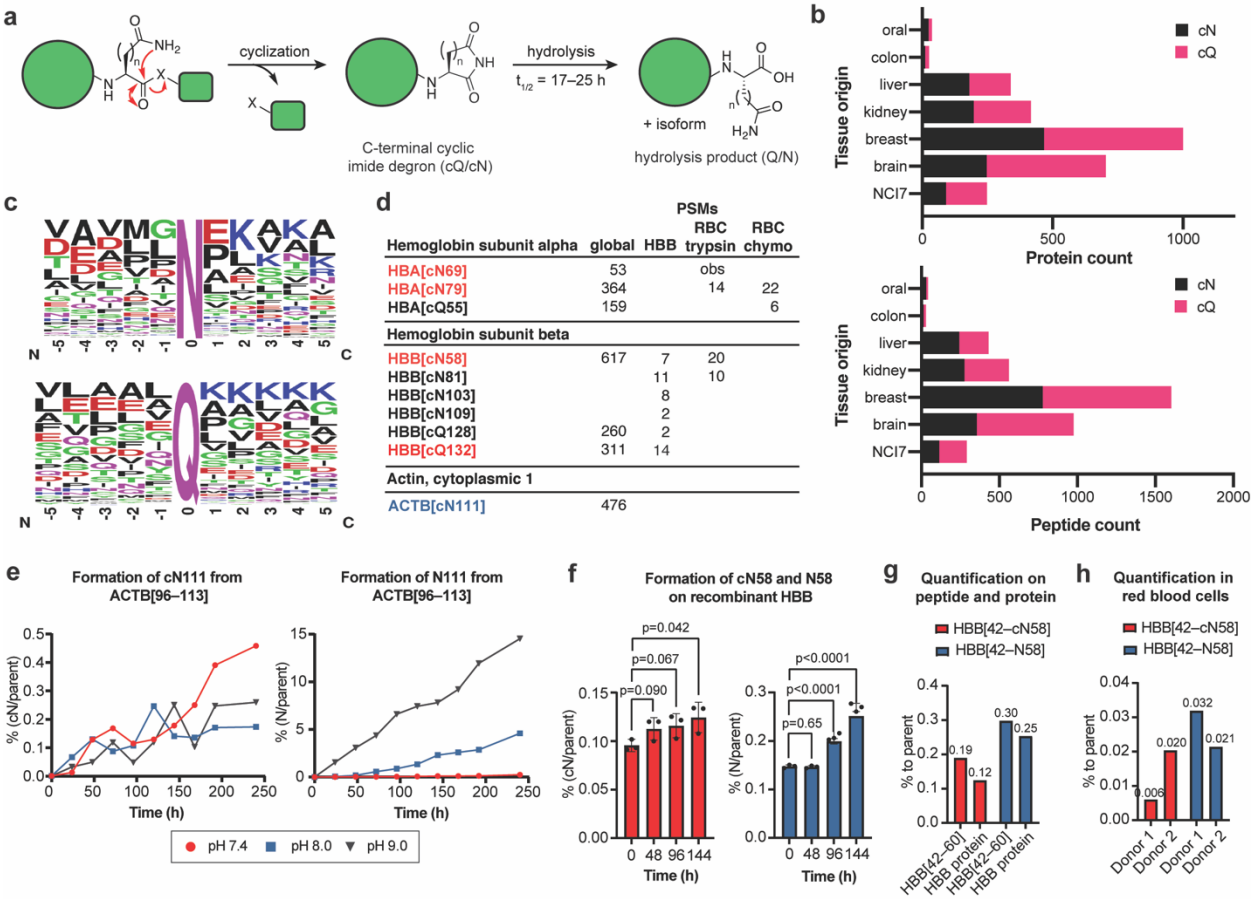

Fig. 4. C-Terminal cyclic imides are overlooked post-translational modifications that form readily in vitro. (**a**) Schematic of cyclic imide formation, which reveals a degron for CRBN, and the subsequent hydrolysis product. (**b**) Unique proteins and peptides that have at least one cN or cQ modification from CPTAC global proteomics datasets. (**c**) Frequency chart of the sequence alignment flanking the –5 to +5 amino acids surrounding cN and cQ sites observed in CPTAC datasets. Alignment generated by weblogo.berkeley.edu. (**d**) Comparison of peptide spectral matches (PSMs) for selected hemoglobin subunits and actin observed in global proteomics datasets, recombinant hemoglobin beta (HBB) protein, and red blood cell (RBC) lysates. HBA[63–cN69] was observed by extracted ion chromatogram in the MS1. Sites selected for further analysis are highlighted in red or blue. (**e**) In vitro time course for formation of ACTB[96–cN111] and ACTB[96–N111] from the synthetic peptide representing ACTB[96–113]. (**f**) In vitro time course for formation of HBB[42–cN58] and HBB[42–N58] on full-length recombinant HBB protein. Experiments were performed in triplicate and quantification was performed by selected ion monitoring. Comparisons were performed using an unpaired two-tailed t-test and p-values are noted. (**g**) Quantification of HBB[42–cN58] and HBB[42–N58] on HBB[42–60] peptide and recombinant HBB protein after 144 h incubation. (**h**) Quantification of HBB[42–cN58] and HBB[42–N58] by selected ion monitoring in two RBC donors.

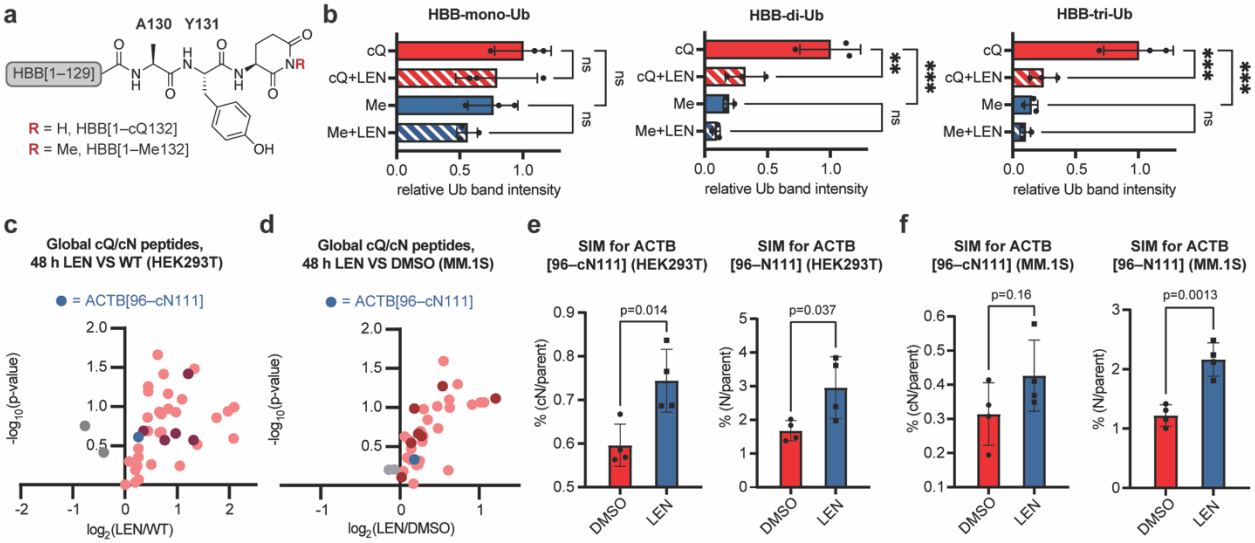

Fig. 5. CRBN regulates recombinant and endogenous substrates bearing C-terminal cyclic imides. (**a**) Schematic of HBB[1–cQ132] and its methylated derivative HBB[1–Me132]. HBB[1–cQ132] = HBB native sequence with C-terminal glutarimide at residue 132 instead of glutamine. (**b**) Quantification of mono-, di-, and tri-mono-ubiquitinated HBB band intensity from in vitro ubiquitination of HBB[1–cQ132] or HBB[1–Me132] with K0 ubiquitin. Comparisons were performed using an ordinary one-way ANOVA with Šídák's multiple comparisons test. ns = not significant, * = $p < 0.05$, ** = $p < 0.01$, *** = $p < 0.001$, **** = $p < 0.0001$. (**c**) Volcano plot of peptide groups bearing C-terminal cyclic imides in HEK293T treated without or with 200 µM lenalidomide over 48 h. Upregulated proteins at 1% FDR = red, 5% FDR = pink. ACTB[96–cN111] peptide = blue. (**d**) Volcano plot of peptide groups bearing C-terminal cyclic imides in MM.1S treated with DMSO or 200 µM lenalidomide over 48 h. Upregulated proteins at 1% FDR = red, 5% FDR = pink. ACTB[96–cN111] peptide = blue. (**e–f**) Quantification of ACTB[96–cN111] and ACTB[96–N111] in HEK293T (**e**) and MM.1S (**f**) treated with DMSO or 200 µM lenalidomide over 48 h using selected ion monitoring (SIM). Comparisons were performed using an unpaired two-tailed t-test and p-values are noted.

Extended Data Figures

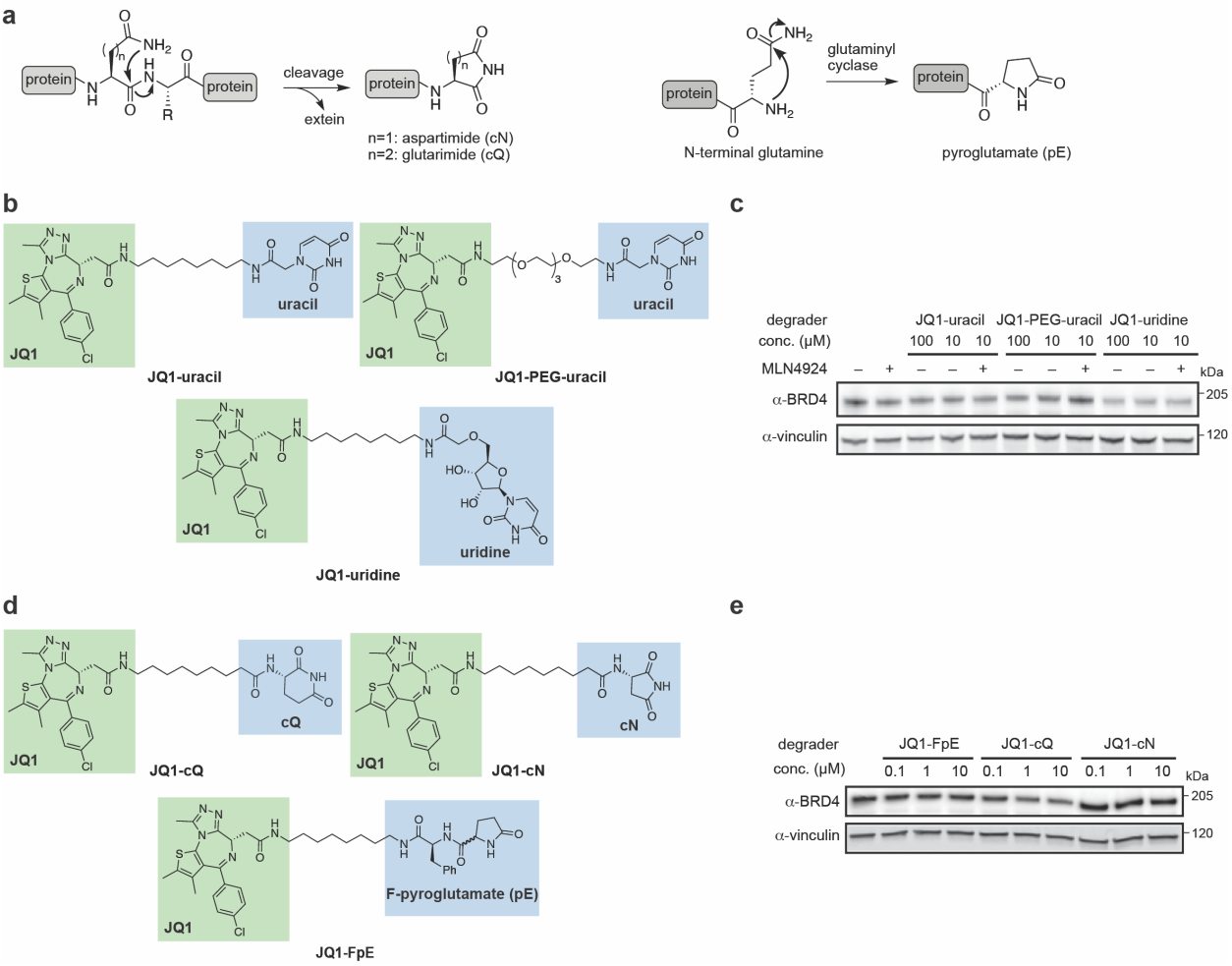

Extended Data Fig. 1. Examination of bifunctional degraders of BRD4 with candidate degrons for CRBN. (**a**) Representative mechanisms of the formation of C-terminal cyclic aspartimide (cN) or glutarimide (cQ) and N-terminal pyroglutamate (pE) in vivo. (**b**) Structures of JQ1-uracil, JQ1-PEG-uracil, and JQ1-uridine. (**c**) Western blot of BRD4 after treatment with JQ1-uracil, JQ1-PEG-uracil, JQ1-uridine in HEK293T cells for 24 h. (**d**) Structures of JQ1-cQ, JQ1-cN, and JQ1-FpE. (**e**) Western blot of BRD4 after treatment with JQ1-cQ, JQ1-cN, JQ1-FpE in HEK293T cells for 4 h. All western blot data are representative of at least 2 independent replicates. For uncropped western blot images, see Supplementary Figure 8.

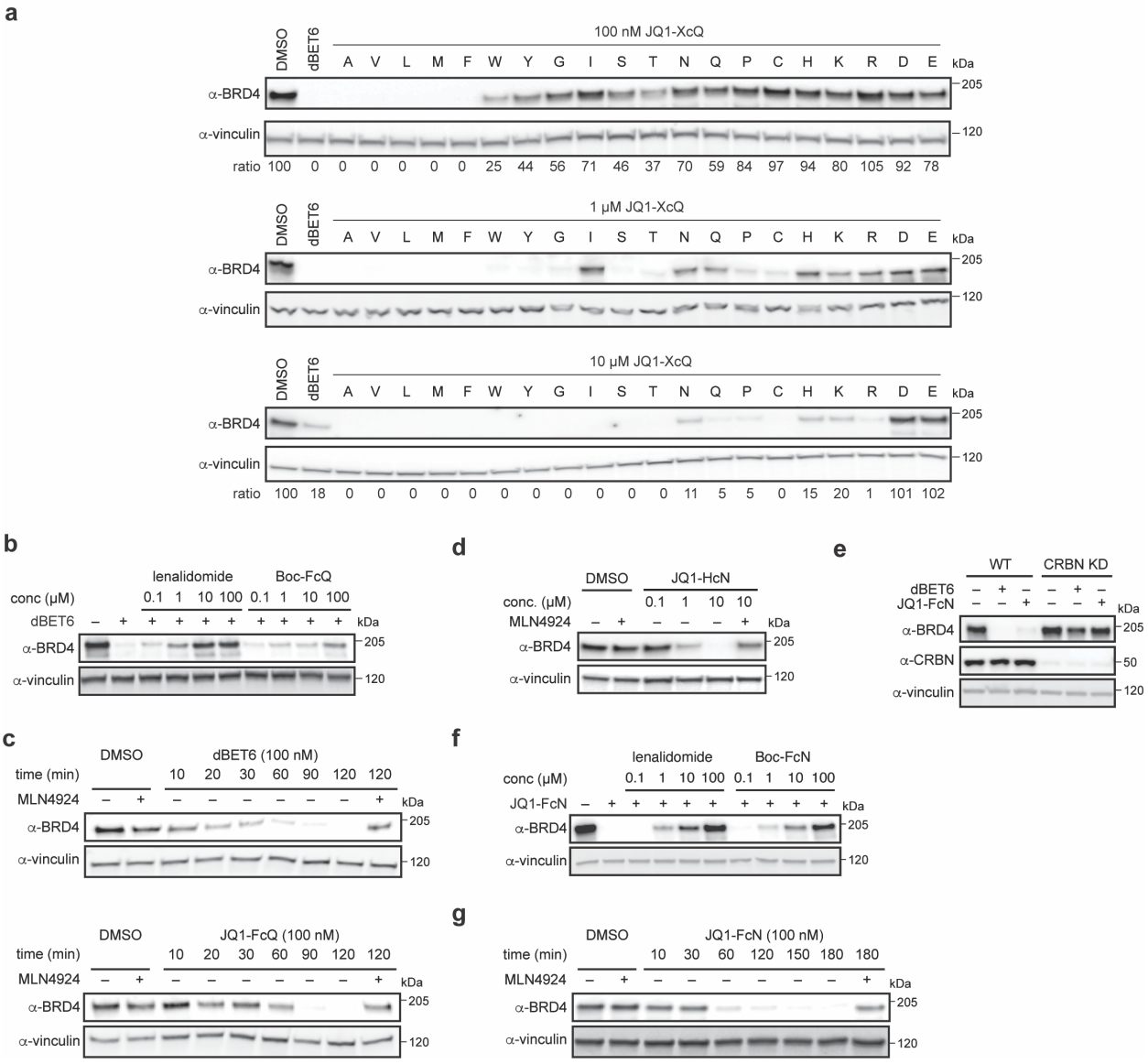

Extended Data Fig. 2. Evaluation of JQ1-XcQ and JQ1-XcN degraders in targeted protein degradation of BRD4. (**a**) Western blots of BRD4 levels after treatment of HEK293T cells with 100 nM, 1 μM, or 10 μM dBET6 for the 20 dipeptide degraders. (**b**) BRD4 degradation with dBET6 over 4 h was competitively inhibited by lenalidomide or Boc-FcQ over a dose-dependent concentration (0.1–100 μM). (**c**) Levels of BRD4 over time in HEK293T cells treated with dBET6 or JQ1-FcQ. (**d**) Evaluation of JQ1-HcN in targeted protein degradation of BRD4 at various concentrations in HEK293T cells over 4 h. (**e**) Western blot of BRD4 after treatment of wild type (WT) or shRNA knockdown (CRBN KD) HEK293T cells with the indicated degrader. (**f**) Western blot of BRD4 after co-treatment of HEK293T cells with JQ1-FcN and lenalidomide or Boc-FcN. (**g**) Levels of BRD4 over time in HEK293T cells treated with JQ1-FcN. All western blot data are

representative of 2 independent replicates. For uncropped western blot images, see Supplementary Figure 8.

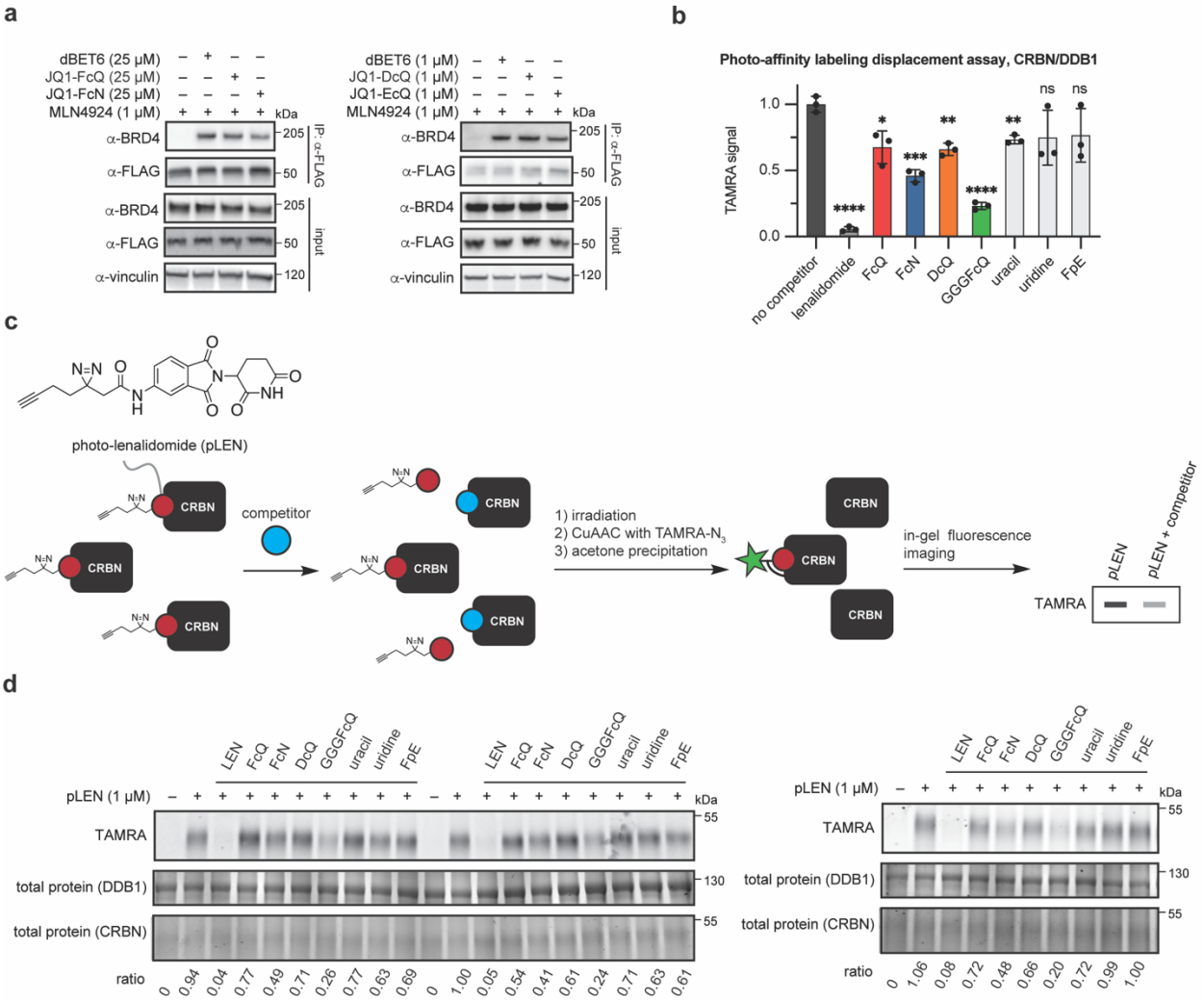

Extended Data Fig. 3. Co-immunoprecipitation and photo-affinity displacement assay with dipeptide degraders and ligands. (**a**) Co-immunoprecipitation of endogenous BRD4 from HEK-CRBN in cells (left) or in lysates (right) after 2 h treatment with 25 µM or 1 µM of the indicated degrader. Western blot data are representative of 2 independent replicates. (**b**) Photo-affinity labeling displacement assay using photo-lenalidomide (pLEN) to visualize in-gel fluorescence imaging of CRBN/DDB1. Comparisons were performed using unpaired two-tailed t-tests. ns = not significant, * = $p < 0.05$, ** = $p < 0.01$, *** = $p < 0.001$, **** = $p < 0.0001$. (**c**) Structure of photo-lenalidomide (pLEN) and schematic of photo-affinity labeling displacement assay using photo-lenalidomide (pLEN) to visualize in-gel fluorescence imaging of CRBN/DDB1. (**d**) Corresponding gel images after treatment of CRBN/DDB1 with 1 µM pLEN and 100 µM of the indicated competitor for 30 min prior to photo-affinity labeling and in-gel fluorescence imaging. For uncropped western blot and gel images, see Supplementary Figure 9.

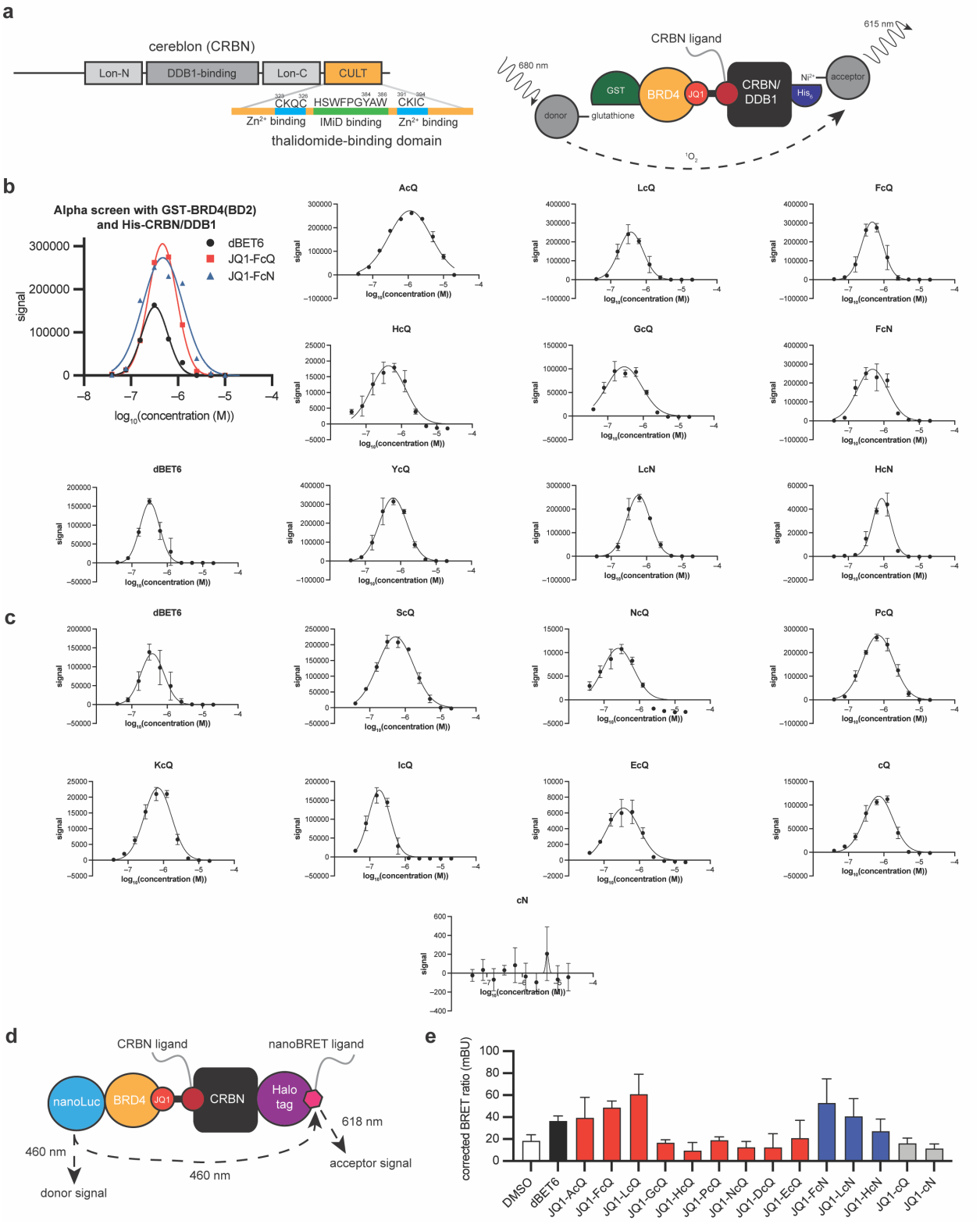

Extended Data Fig. 4. Ternary complex formation of dipeptide ligands with CRBN and BRD4. (**a**) Schematic showing the domains of CRBN, including the CULT domain with key residues for immunomodulatory drug binding highlighted, and AlphaScreen design. (**b**–**c**)

Alphascreen experiments performed with the indicated degrader compounds. Data shown in (**b**) and (**c**) are each performed on a single 384-well plate; dBET6 was assayed on each plate as an internal control. Each condition was measured in triplicate. (**d**) Schematic of NanoBRET assay. (**e**) NanoBRET measurement of ternary complex formation induced by the indicated members of the degrader library as determined by acceptor:donor signal ratio, with background signal from no-ligand control for each degrader subtracted. Each condition was assayed in triplicate. Error bars represent SEM.

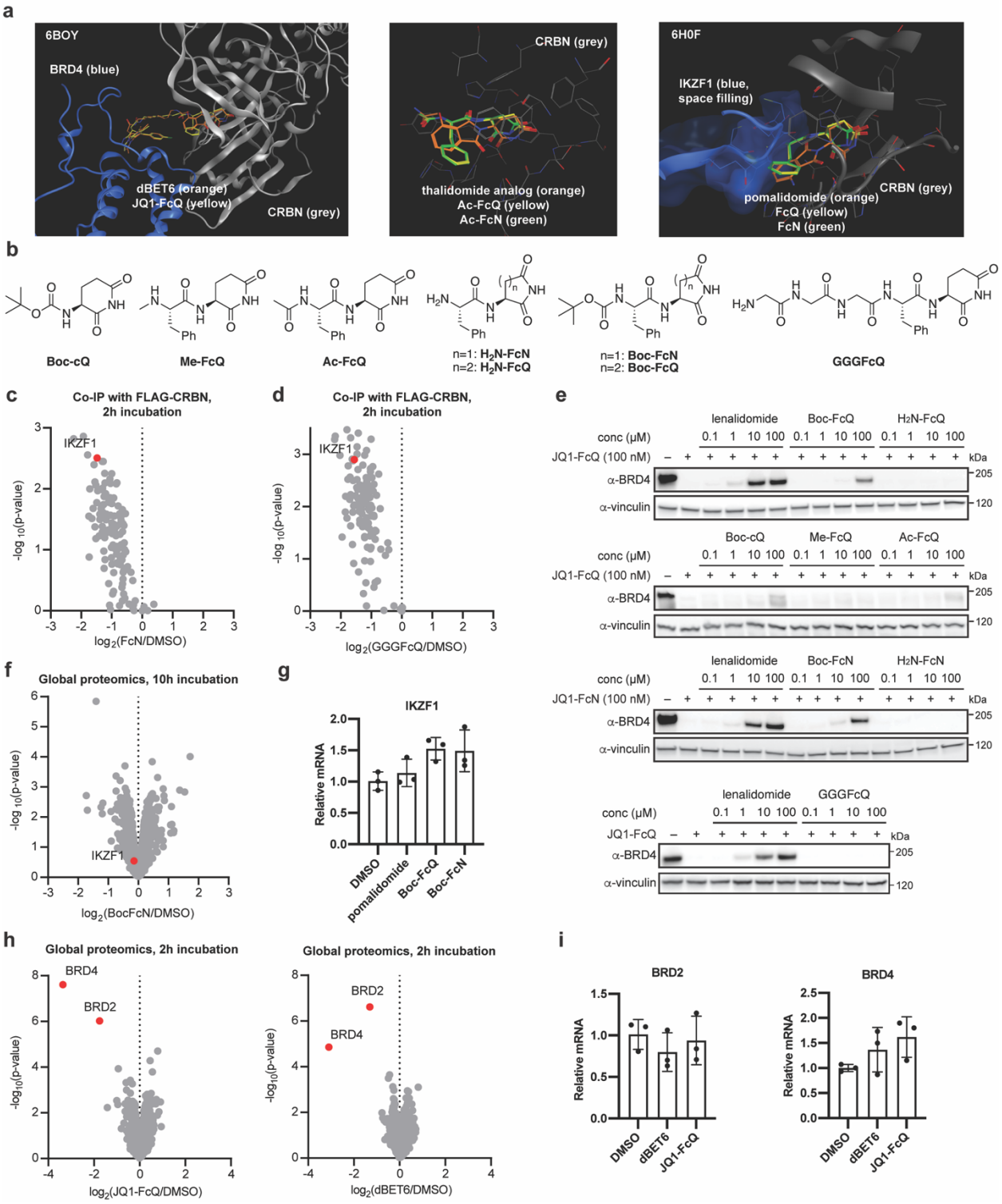

Extended Data Fig. 5. Characterization of the IMiDs and the indicated peptides in HEK293T cells and multiple myeloma MM.1S cells. (**a**) Model of dipeptide degraders with CRBN built from 6BOY and 6H0F. Left: Model of JQ1-FcQ (yellow) by molecular modeling of dBET6 (orange) in the ternary complex with CRBN (grey) and BRD4 (blue). Middle: zoom-in of the CRBN binding pocket with thalidomide analog (orange), Ac-FcQ (yellow), or Ac-FcN (green).

Right: Model of pomalidomide (orange), FcQ (yellow), and FcN (green) in the ternary complex with CRBN (grey) and IKZF1 (blue, space-filling mode). (**b**) Structures of Boc-cQ, Me-FcQ, Ac-FcQ, H_2N-FcN or H_2N-FcQ, Boc-FcN or Boc-FcQ, and GGGFcQ. (**c–d**) Quantitative proteomics of co-immunoprecipitated proteins from lysates of HEK-CRBN cells overexpressing IKZF1 after 2 h incubation with 1 μM (**c**) FcN or (**d**) GGGFcQ. Protein levels were normalized to the amount of CRBN in each channel. (**e**) Competitive inhibition of BRD4 degradation by the indicated dipeptide degrader (JQ1-FcN, JQ1-FcQ) with the indicated compounds in HEK293T cells for 4 h. (**f**) Quantitative proteomics of MM.1S cells after treatment with 10 μM of Boc-FcN for 10 h. (**g**) Protein expression levels of IKZF1 after treatment with the indicated compounds in MM.1S cells for 10 h. (**h**) Quantitative proteomics of HEK293T cells after treatment with 0.1 μM of JQ1-FcQ or dBET6 for 2 h. (**i**) Protein expression levels of BRD2 and BRD4 after treatment with the indicated compounds in HEK293T cells for 2 h. All proteomics experiments were performed in triplicates. For uncropped western blot images, see Supplementary Figure 10.

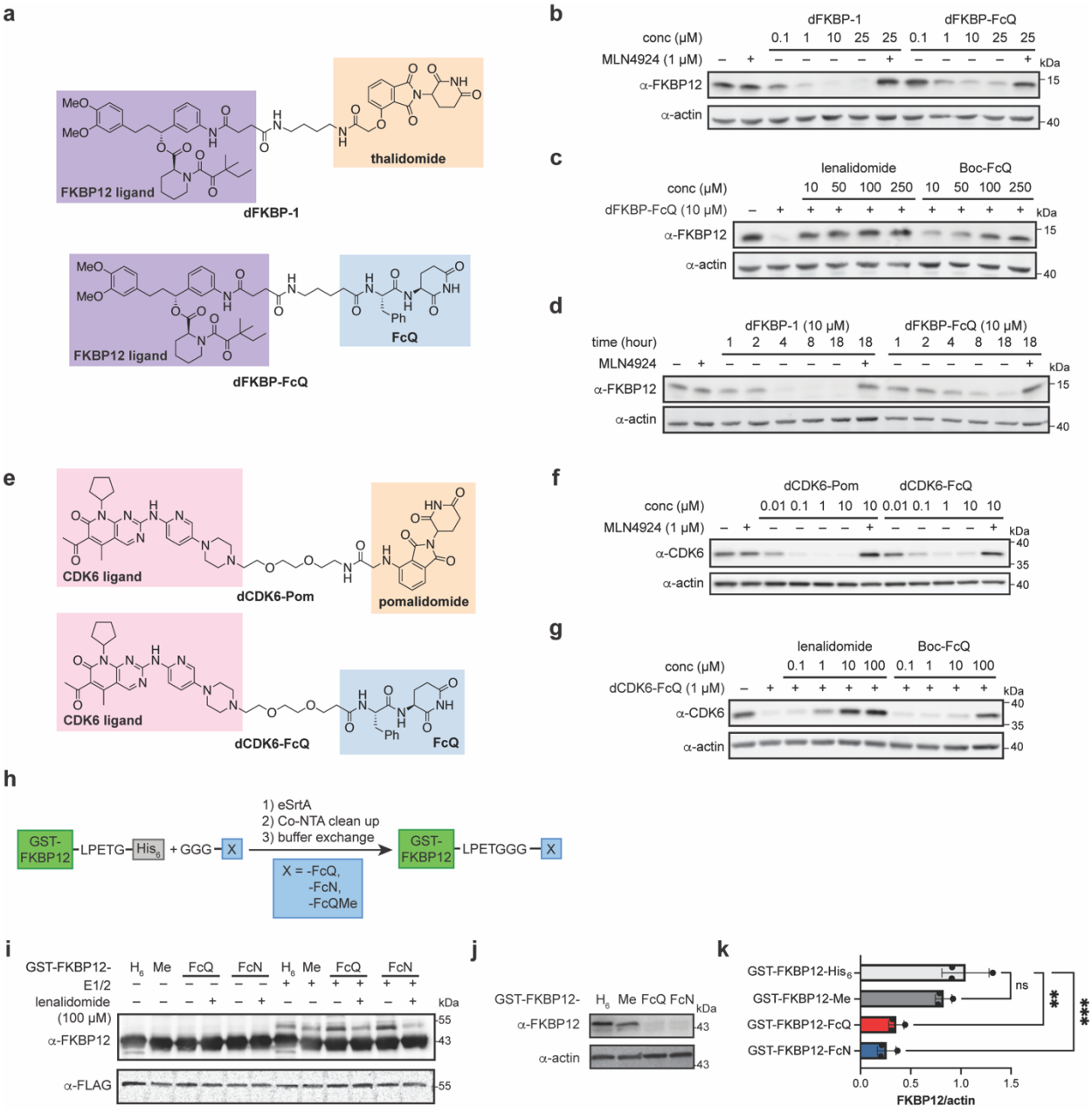

Extended Data Fig. 6. The C-terminal cyclic imide degron is transferrable. (**a**) Structure of FKBP12 degraders dFKBP-1 and dFKBP-FcQ. (**b**) Western blot of FKBP12 levels after treatment of HEK293T cells with dFKBP-1 or dFKBP-FcQ over a 0.1–25 μM dose-response range. (**c**) Western blot of FKBP12 levels after co-treatment of HEK293T cells with dFKBP-FcQ and lenalidomide or Boc-FcQ. (**d**) Levels of FKBP12 over time in HEK293T cells treated with dFKBP-1 or dFKBP-FcQ. (**e**) Structure of CDK6 degraders dCDK6-Pom and dCDK6-FcQ. (**f**) Western blot of CDK4/6 levels after treatment of Jurkat cells with dCDK6-Pom or dCDK6-FcQ over a 0.01–10 μM dose-response range. (**g**) Western blot of CDK6 levels after co-treatment of Jurkat cells with dCDK6-FcQ and lenalidomide or Boc-FcQ. (**h**) Sortase system used to generate degron-tagged GST-FKBP12 from GST-FKBP12-LPETG-His_6. (**i**) In vitro ubiquitination of FKBP12 tagged with C-terminal cyclic imide. FKBP12-H_6 = FKBP12 with C-terminal His_6 tag (no sortase

treatment); FKBP12-Me = FKBP12 with C-terminal FcQMe; FKBP12-FcQ = FKBP12 with C-terminal FcQ; FKBP12-FcN = FKBP12 with C-terminal FcN. (**j**) Western blot of FKBP12 tagged with the indicated peptides 6 h after electroporation into HEK293T cells. (**k**) Quantification of Western blot in (**j**). Comparisons were performed using an ordinary one-way ANOVA with Šídák's multiple comparisons test. ns = not significant, * = $p < 0.05$, ** = $p < 0.01$, *** = $p < 0.001$, **** = $p < 0.0001$. All western blot data are representative of at least 2 independent replicates. Flow cytometry data is representative of 3 independent replicates. For uncropped western blot images, see Supplementary Figure 10.

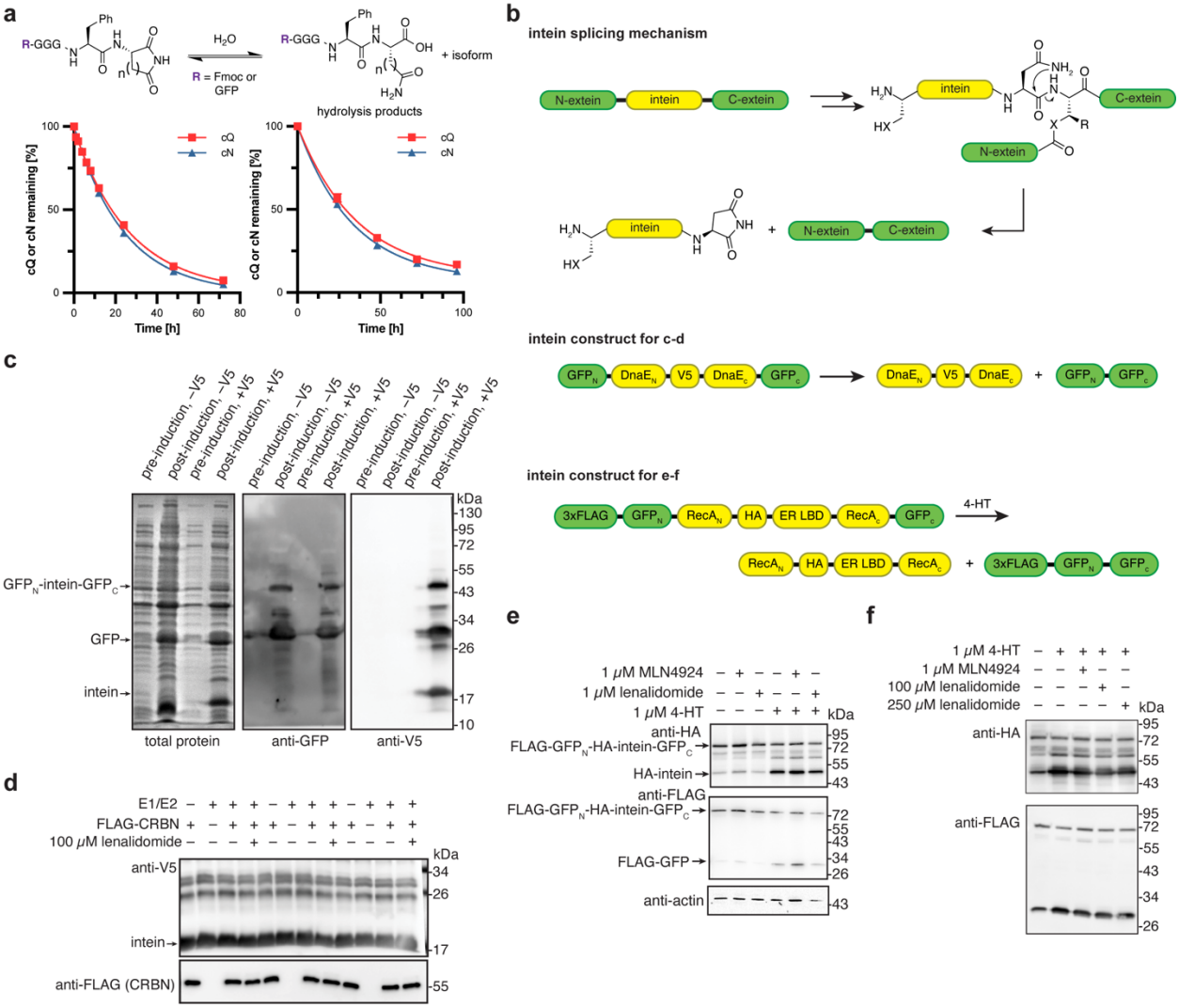

Extended Data Fig. 7. The inteins Npu DnaE and Mtu RecA are not CRBN substrates. (**a**) Left: hydrolysis of cyclic imides Fmoc-GGGFcQ or Fmoc-GGGFcN in PBS at 37 °C. Right: hydrolysis of C-terminal cyclic imides on GFP-FcQ or GFP-FcN in PBS at 37 °C. (**b**) Schematic of the intein splicing mechanism with the penultimate step in intein excision that generates a C-terminal aspartimide highlighted, and the two intein constructs before and after splicing. X = O or S, R = H or CH_3. (**c**) Analysis of expression and splicing of Npu DnaE in E. coli with and without a V5 tag inserted in the intein. (**d**) In vitro ubiquitination of V5-tagged cell lysate generated in **c**. (**e**, **f**) Effect of MLN4924 or lenalidomide pretreatment on 4-hydroxytamoxifen (4-HT)–induced splicing of GFP with HA-tagged Mtu RecA intein in HEK293T cells. For uncropped western blot images, see Supplementary Figure 11.

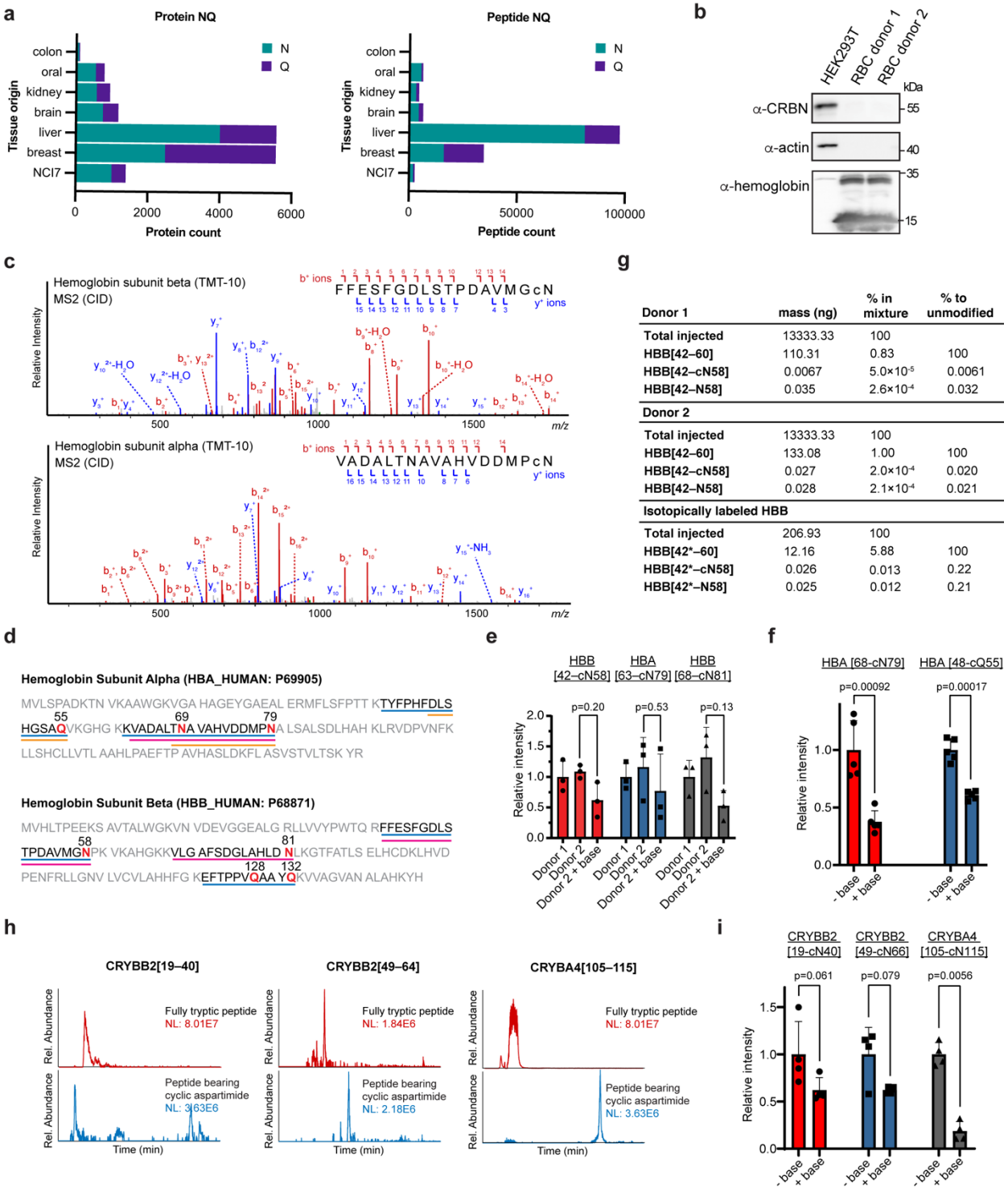

Donor 1	mass (ng)	% in mixture	% to unmodified
Total injected	13333.33	100	
HBB[42–60]	110.31	0.83	100
HBB[42–cN58]	0.0067	5.0×10^{-5}	0.0061
HBB[42–N58]	0.035	2.6×10^{-4}	0.032
Donor 2			
Total injected	13333.33	100	
HBB[42–60]	133.08	1.00	100
HBB[42–cN58]	0.027	2.0×10^{-4}	0.020
HBB[42–N58]	0.028	2.1×10^{-4}	0.021
Isotopically labeled HBB			
Total injected	206.93	100	
HBB[42*–60]	12.16	5.88	100
HBB[42*–cN58]	0.026	0.013	0.22
HBB[42*–N58]	0.025	0.012	0.21

Extended Data Fig. 8. Analysis of C-terminal cQ/cN modifications on hemoglobin derived from red blood cells and beta-crystallin derived from bovine lens. (**a**) Unique proteins and peptides that carry a semi-tryptic terminal N or Q from global proteomics datasets. (**b**) Western blot of red blood cell (RBC) lysates from two donors in comparison to HEK293T lysate. RBCs do not express CRBN. (**c**) Representative MS2 spectra of HBB[42–cN58] and HBA[63–cN79]

detected in RBC lysates. (**d**) Schematic of the sequences of hemoglobin subunits alpha and beta. The peptides with cN modifications observed by trypsin or chymotrypsin digestion and MS analysis are underlined (global datasets = blue, RBC tryptic peptides = pink, RBC chymotryptic peptides = orange) and the modification sites are highlighted in red. (**e**) Quantification of the three major peptide groups bearing a C-terminal cyclic imide from RBC samples with or without base treatment. The experiment was performed in biological triplicate and the noted p-values were obtained by one-way ANOVA with TukeyHSD post-hoc test from Proteome Discoverer. (**f**) Quantification of the two major chymotryptic peptide groups bearing C-terminal cyclic imides in RBC samples with or without base treatment. The experiment was performed in biological quintuplicate and the noted p-values were obtained by one-way ANOVA with TukeyHSD post-hoc test from Proteome Discoverer. (**g**) Quantification of the absolute masses and percentages of HBB[42–60], HBB[42–cN58], and HBB[42–N58] in RBC samples using selected ion monitoring. (**h**) Ion intensity chromatograms extracted for the masses of the cyclic imide fragment and the corresponding tryptic peptide for three cyclic imide-bearing peptide groups identified in bovine lens. (**i**) Quantification of these peptide groups validates the sensitivity of the cyclic imide modifications to base treatment. The experiment was performed in biological quadruplicate and the noted p-values were obtained by one-way ANOVA with TukeyHSD post-hoc test from Proteome Discoverer. For uncropped western blot images, see Supplementary Figure 11.

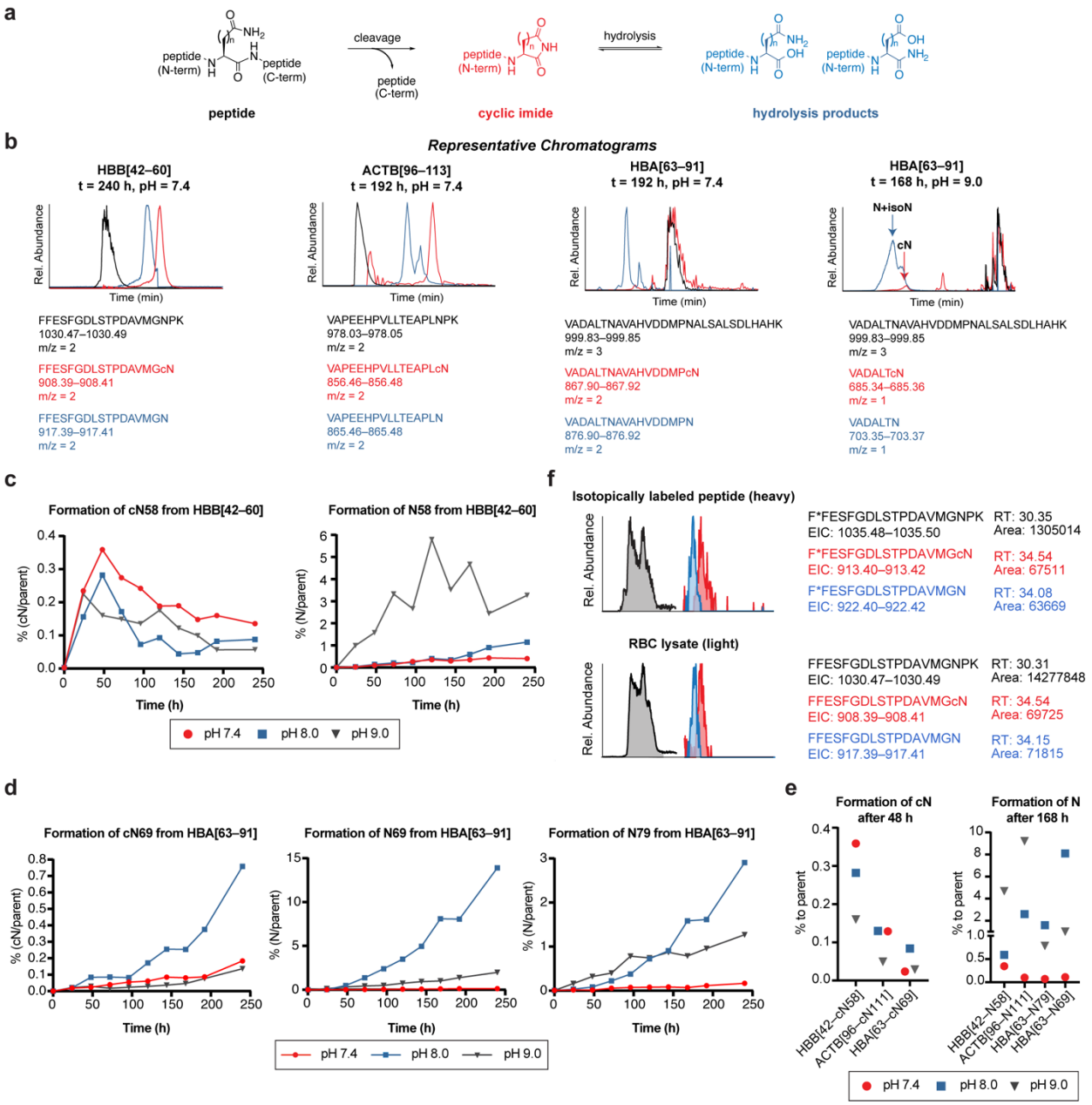

Extended Data Fig. 9. Analysis of C-terminal cQ/cN and Q/N modifications on synthetic peptides. (**a**) Scheme of cyclic imide formation in a peptide and subsequent hydrolysis to afford the truncated C-terminal glutamine or asparagine fragments. (**b**) Overlay of representative extracted ion chromatograms of each peptide at the masses corresponding to parent peptide (black), cyclic imide fragment (red), and its hydrolyzed products (blue). The two constitutional isomers formed via hydrolysis of the cyclic imide fragment were not distinguished in our study. (**c–d**) In vitro time course for formation of the cyclic imide fragment and the hydrolysis products at the indicated position on the synthetic peptide after incubation. (**e**) Percentage of the formed cyclic imide fragment and the hydrolysis products at the indicated residue relative to the parent synthetic peptide at different pH. (**f**) Ion intensity chromatogram extracted for the masses of the corresponding species for RBC lysates and the mixture of isotopically labeled HBB[42*–60]

containing the modifications. The RBC samples were spiked with the peptide mixture and ran on the selected ion monitoring mode to validate the overlap of retention times and amplify the signal of selected ions.

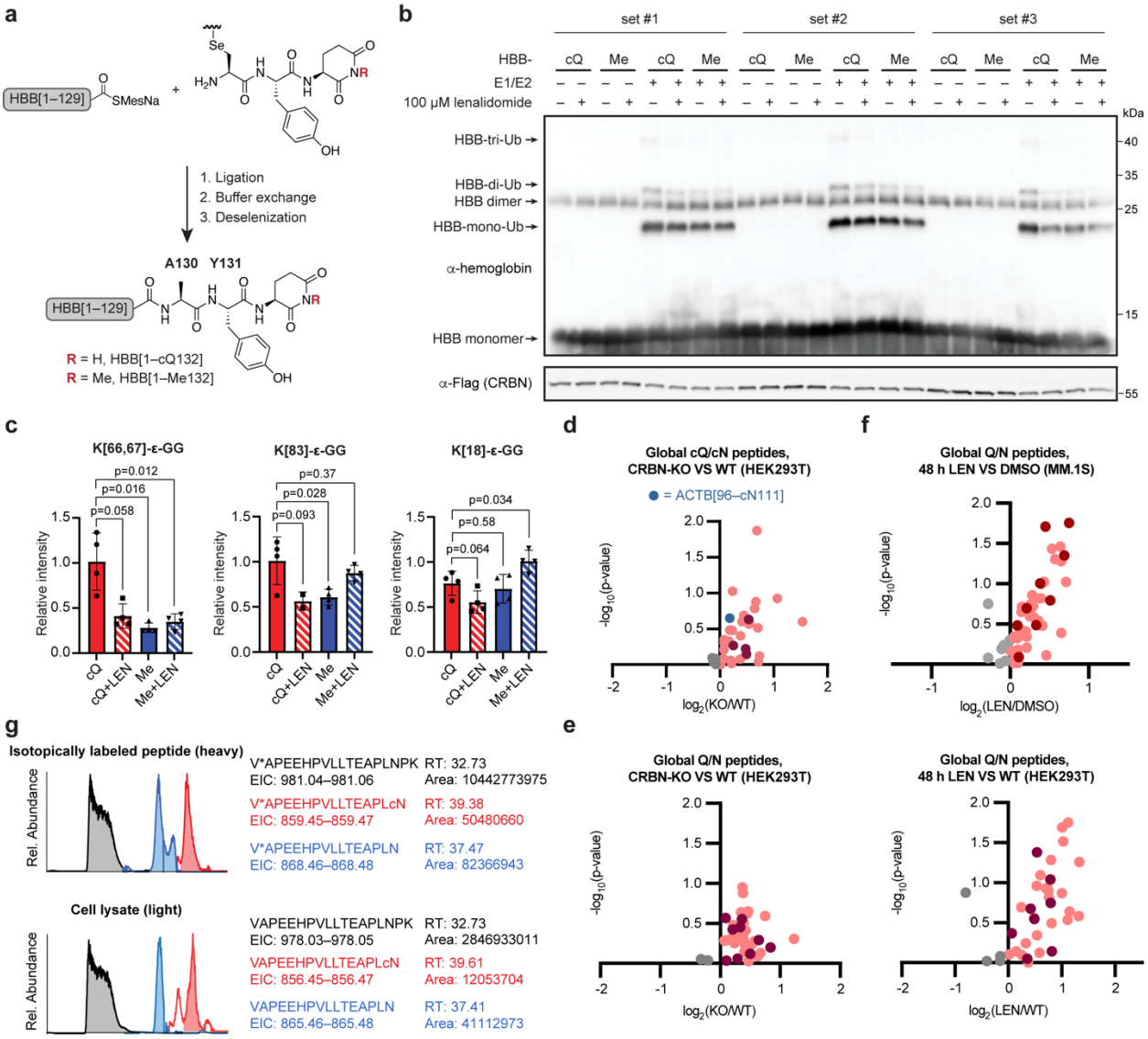

Extended Data Fig. 10. Analysis of substrates bearing C-terminal cQ/cN and Q/N modifications in vitro and in cells. (**a**) Schematic of expressed protein ligation using HBB[1–129] thioester and Sec-YcQ or Sec-YcQMe to generate HBB[1–cQ132] or HBB[1–Me132]. (**b**) Western blot of in vitro ubiquitination of HBB proteins in triplicate. (**c**) TMT-based quantification of K-ε-GG sites identified from the in vitro ubiquitination samples using mass spectrometry. The experiment was performed in technical quadruplicate and comparisons were performed using unpaired two-tailed t-tests and p-values are noted. (**d**) Volcano plots of peptide groups bearing C-terminal cyclic imides in WT HEK293T or CRBN CRISPR/Cas9 knockout HEK293T over 48 h. Upregulated proteins at 1% FDR = red, 5% FDR = pink. ACTB[96–cN111] peptide = blue. (**e**) Volcano plots of peptide groups bearing C-terminal glutamine or asparagine (protein terminus excluded) in WT HEK293T, CRBN KO HEK293T, or HEK293T treated with 200 μM lenalidomide over 48 h. Upregulated peptide groups at 1% FDR = red, 5% FDR = pink. (**f**) Volcano plots of peptide groups bearing C-terminal glutamine or asparagine (protein terminus excluded) in MM.1S treated with DMSO or 200 μM lenalidomide over 48 h. Upregulated peptide groups at 1% FDR = red, 5% FDR = pink. (**g**) Ion intensity chromatogram extracted for the masses of the

corresponding species for HEK293T lysates and the mixture of isotopically labeled ACTB[96*–113] containing the modifications. The cell samples were spiked with the peptide mixture and ran on the selected ion monitoring mode to validate the overlap of retention times and amplify the signal of selected ions. For uncropped western blot images, see Supplementary Figure 11.